Transportation Research Part B 173 (2023) 203–227

Contents lists available at ScienceDirect

Transportation Research Part B

journal homepage: www.elsevier.com/locate/trb

Non-unimodal and non-concave relationships in the network Macroscopic Fundamental Diagram caused by hierarchical streets

Guanhao Xu [a,1], Vikash V. Gayah [b,*]

[a] Buildings and Transportation Science Division, Oak Ridge National Laboratory, Knoxville, TN, 37932, USA
[b] Department of Civil and Environmental Engineering, The Pennsylvania State University, University Park, PA, 16802, USA

ARTICLE INFO

Keywords:
Macroscopic fundamental diagram
Hierarchical street network
User equilibrium
System optimal
Non-unimodal

ABSTRACT

Unimodal, concave relationships between average network productivity and accumulation or density aggregated across spatially compact regions of urban networks—so called network Macroscopic Fundamental Diagrams (MFDs)—have recently been shown to exist on homogeneous street networks. When present, MFD relationships facilitate the modeling of traffic congestion at a regional level and have led to the development of various regional traffic control strategies. However, real street networks are not homogeneous—they generally have a hierarchical structure where some streets (e.g., arterials) promote higher mobility than others (e.g., local roads). This paper examines how the presence of hierarchical roadway structures may potentially cause non-unimodal patterns in a network's MFD. These are observed using three types of tools: analytical models of simple network structures, simulations of various idealized roadway networks, and empirical data. The impacts of street hierarchy depend on how vehicles use different roadway types to move within the network; i.e., their routing strategy. The findings suggest that the presence of roadway hierarchies may lead to MFDs that have non-unimodal or non-concave patterns on the free-flow branch when vehicles route themselves according to user equilibrium principles, which is closest to what would be observed in realistic situations. Such patterns are contrary to what is traditionally assumed in most MFD-based modeling frameworks. However, the unimodal and concave MFD should be expected under system optimal routing conditions that maximize network productivity for a given traffic state.

1. Introduction

Although aggregate (network-wide) traffic relationships have been studied intermittently for nearly 50 years (Godfrey, 1969; Mahmassani et al., 1984, 1987), recent empirical confirmation of well-defined relationships just over a decade ago (Geroliminis and Daganzo, 2008) has led to a renewed interest in this topic. Geroliminis and Daganzo (2008) showed that a unimodal, concave relationship exists between the average productivity and accumulation/density of vehicles traveling on a network using data from Yokohama, Japan. Such relationships are commonly referred to as network Macroscopic Fundamental Diagrams or (flow-)MFDs.

* Corresponding author.
E-mail address: gayah@engr.psu.edu (V.V. Gayah).

[1] This manuscript has been authored in part by UT-Battelle, LLC, under contract DE-AC05-00OR22725 with the US Department of Energy (DOE). The publisher acknowledges the US government license to provide public access under the DOE Public Access Plan (http://energy.gov/downloads/doe-public-access-plan).

https://doi.org/10.1016/j.trb.2023.05.002
Received 30 July 2021; Received in revised form 2 May 2023; Accepted 5 May 2023
Available online 12 May 2023

Another study showed how the existence of a flow-MFD also implies the existence of a relationship between the rate at which trips can be completed in a network and accumulation/density of vehicles within the network (Daganzo, 2007). This latter relationship is commonly known as the Network Exit Function or outflow-MFD. In this study, we will focus on the flow-MFD (abbreviated as MFD in the rest of the paper). When present, MFDs can be used to model traffic dynamics within an urban network by dividing the network into a set of spatially compact homogeneous regions and tracking the average level of congestion in each (Daganzo, 2007). Many studies have examined situations or properties that are necessary for well-defined MFDs to exist (Daganzo et al., 2011; Geroliminis and Sun, 2011; Knoop and Hoogendoorn, 2013; Mazloumian et al., 2010; Saberi et al., 2014). A variety of regional traffic control studies have been developed using this MFD-based representation of urban traffic networks; recent relevant examples in the literature include perimeter metering control (Aboudolas and Geroliminis, 2013; Geroliminis et al., 2013; Haddad, 2017; Haitao et al., 2019; Keyvan-Ekbatani et al., 2013, 2012; Ren et al., 2020; Yildirimoglu et al., 2018), pricing (Gonzales and Daganzo, 2013, 2012; Gu et al., 2018; Loder et al., 2022; Simoni et al., 2015; Yang et al., 2019; Zheng et al., 2016, 2012) and street network design (Deprator et al., 2017; Ortigosa et al., 2019). A thorough review of the history of macroscopic modeling of urban networks is provided in (Johari et al., 2021). However, we focus here on the estimation of a network's MFD and theoretical relationships between network properties and the functional form of an MFD, since this is the focus of this paper.

Various studies have proposed methods to estimate a network's MFD using loop detector data (Ambühl et al., 2021, 2019; Ampountolas and Kouvelas, 2015; Buisson and Ladier, 2009; Li et al., 2022; Wang et al., 2015), floating car data (Bazzani et al., 2011; Huang et al., 2019; Ji et al., 2014; Knoop et al., 2018; Paipuri et al., 2021, 2020; Shim et al., 2019; Tsubota et al., 2014), or a combination of both (Ambühl and Menendez, 2016; Du et al., 2016; Fu et al., 2020; Geroliminis and Daganzo, 2008; Hong et al., 2022; Leclercq et al., 2014; Loder et al., 2017; Nagle and Gayah, 2014; Saffari et al., 2022, 2020). This is not a trivial task as a tremendous amount of data is generally needed for MFD estimation, and there are issues when estimating an MFD empirically using traditional data sources. For example, MFDs derived from loop detector data generally overestimate densities due to standing queues at intersections and can be significantly biased depending on the loop detector distribution over the networks (Courbon and Leclercq, 2011). Moreover, scattered plots may also be observed when traffic conditions are not homogeneous within the network (Leclercq et al., 2014). MFDs derived from floating car data are sensitive to the impacts of sampling (Leclercq et al., 2014) and are fairly inaccurate in free-flow states (Gayah and Dixit, 2013). Finally, empirical data does not allow systematic analysis of the characteristics of the MFD and the influential factors on its shape (Tilg et al., 2020).

Analytical methods have also been proposed to estimate a network's MFD as a function of various network properties, such as average block lengths, signal timings, traffic flow characteristics on links, and route choice (Aghamohammadi and Laval, 2022; Daganzo and Geroliminis, 2008; Dakic et al., 2020; Geroliminis and Boyaci, 2012; Hans et al., 2015; Laval and Castrillón, 2015; Leclercq and Geroliminis, 2013; Tilg et al., 2020; Xu et al., 2020). These methods generally abstract a network into a single, infinitely long corridor and apply the variational theory of kinematic waves (Daganzo, 2005; Daganzo and Lehe, 2016; Daganzo and Menendez, 2005; Tilg et al., 2021) to estimate the average flow-density relationship along the corridor. These existing analytical methods can be applied to homogeneous networks made up of similar link types.

Unfortunately, real street networks are not homogeneous—they tend to have a hierarchical structure where some streets promote higher mobility (e.g., arterials) while others promote higher accessibility (e.g., local roads). Very few studies have considered the impacts of street network hierarchy on MFDs. One related study used simulation to examine how MFDs might change when links were removed in a grid network, which might create unintentional hierarchies (Ortigosa and Menendez, 2014). Knoop et al. (2014) examined how various combinations of arterial and local street network patterns may influence the shape of the MFD using simulation. Network structures were generated randomly so they could not be directly compared. Mühlich et al. (2015) used simulation to study flow-density relationships during congestion onset and dissipation when arterial streets were mixed with local streets. However, these previous studies did not provide analytical methods that could be used to explain or determine general features that might arise in MFDs of hierarchical network structures.

In light of this, this paper examines how MFDs might differ on hierarchical street networks. Findings from microscopic simulation and empirical data are used to demonstrate that non-unimodal or non-concave patterns might emerge in MFDs of hierarchical street networks. Analytical investigation of simple network structures—linear corridors and two-dimensional networks— as done in (Daganzo et al., 2011; Gayah et al., 2014; Gayah and Daganzo, 2011) —are then used to verify that this behavior is caused by the network hierarchy and, specifically, how travelers route themselves on the network to minimize their travel time. This analytical work directly builds on a recent study that considers the MFDs of simple networks with route choice (Leclercq and Geroliminis, 2013) by considering features that are specific to hierarchical network structures. The analytical findings are then used to explain patterns observed in both simulated and empirical MFDs. The results contribute to the growing literature on relationships between traffic variables aggregated across large spatial regions and how these relationships are influenced by network features.

The remainder of this paper is organized as follows. First, simulation and empirical evidence of non-unimodal or non-concave MFDs are presented. Then, an analytical investigation of a hierarchical linear corridor is performed to demonstrate why these patterns might be observed. Next, the analytical model is extended to confirm that the expected patterns still arise in two-dimensional networks. This is followed by the validation of the initial observations using the analytical results. Finally, concluding remarks are provided.

2. Impact of roadway hierarchy on the network MFD

In this section, the impact of roadway hierarchy on a network's observed flow-density relationship is examined via both simulations built in AIMSUN and empirical data from London, UK. The remainder of this section first describes the detailed logic of the simulation and the resulting patterns of the flow-density relationship. Then, evidence of a similar pattern observed in an empirical MFD is

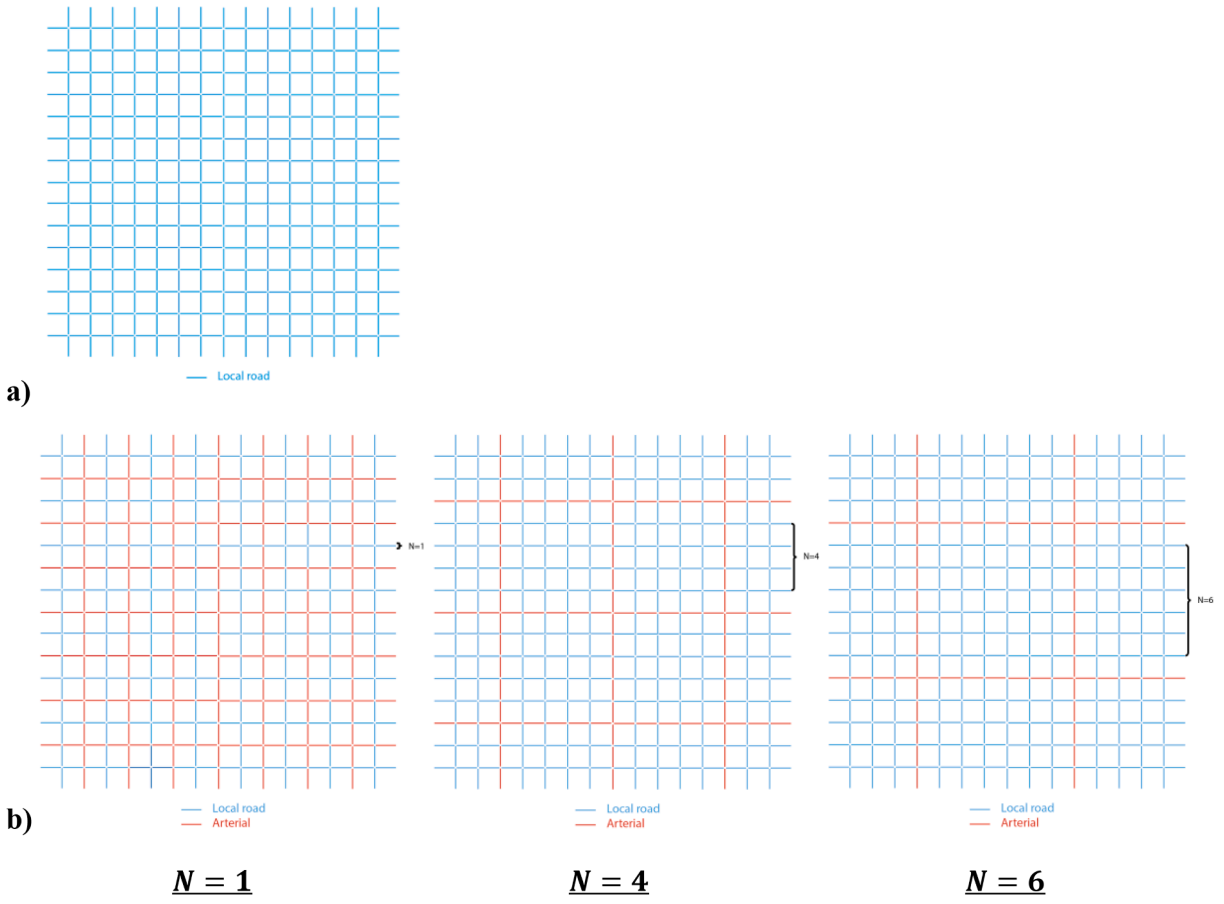

Fig. 1. Simulated network: a) network with no hierarchy; b) grid hierarchical network; c) ring hierarchical network; d) ring-radial hierarchical network.

provided.

2.1. Simulation observations

A simulation of a two-way grid network in AIMSUN is first used to examine the impact of roadway hierarchy on a network's observed flow-density relationship. Four networks are simulated here. The first network has no hierarchy and is composed of two-way local roads arranged into a simple 16×16 square grid pattern, as shown in Fig. 1a. The other three networks are based on the same grid pattern but consist of two types of roads with different properties – e.g., arterials and local streets – and are arranged into different hierarchical structures. In Fig. 1b, arterials and local roads are arranged such that for every $N = 1, \quad 4, \quad 6$ local road, there is 1 arterial. In Fig. 1c, arterials and local roads are arranged into a ring pattern. In Fig. 1d, arterials and local roads are arranged into a ring-radial pattern. Each arterial street consists of two travel lanes with a free flow speed of 50 mile/hr and a capacity of 2400 veh/(lane-hr), while each local street consists of one travel lane which has a common free flow speed of 25 mile/hr and a capacity of 1800 veh/(lane-hr).

In all networks, intersections involving two arterials are signalized. The corresponding signal plan consists of two phases: one for all movements of eastbound and westbound and the other for all movements of northbound and southbound. The signal has a cycle length of 60 s with an equal green time of 26 s, yellow time of 3 s, and all-red time of 1 second provided to both phases. The signal offsets are set to be 0. Intersections involving one arterial and one local road are minor-street stop controlled. The local road is the minor road controlled by a stop sign. Finally, intersections involving two local roads are all-way stop controlled.

The simulation starts with an empty network. Vehicles gradually enter the network with their origins and destinations located at all intersections (for simplicity). Trips are evenly generated between all OD pairs that are horizontally and vertically at least N streets apart, where N is the ratio of the number of local roads to the number of arterials and is set to be an integer. This is done to make sure that arterials will be reasonably considered in the route choice. The demand between each OD pair is at first very low but increases by a fixed value every 1 h until the network is completely congested. This can ensure that all states on the MFD can be observed from the simulation. Finally, the C-logit model embedded in AIMSUN with a scale factor of 5 is used for route choice. The C-logit model is a

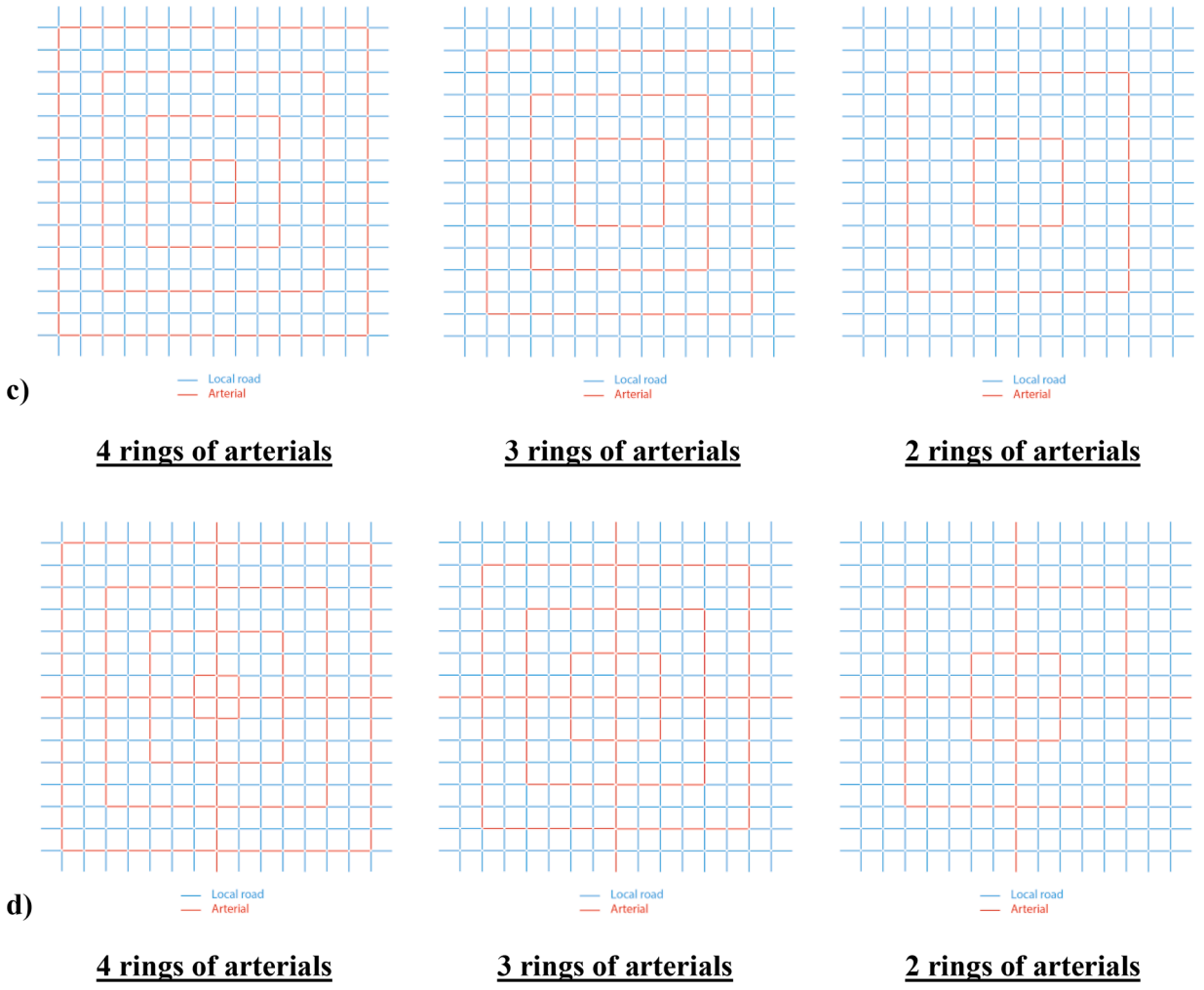

Fig. 1. (*continued*).

modified specification of the Multinomial Logit (MNL) model which can avoid unrealistic choice probabilities for paths sharing a number of links (Cascetta et al., 1996).

Figure 2 provides the observed flow-density relationship of arterials, local roads, and the entire network obtained from the simulations of networks with different network structures. Notice that the MFD for the non-hierarchical network (Fig. 2a) is unimodal, as expected: average flow increases monotonically with density in the free-flow regime of the MFD and plateaus at capacity. However, interestingly, the MFDs of the networks with hierarchical structures (Fig. 2b, c, and d) do not necessarily increase monotonically with network-wide density in the free-flow regime. Instead, the network flow increases with the network density to some value, remains unchanged (or even decreases slightly) as the density increases, and finally increases with network density again until the capacity is reached. This non-unimodal pattern can be generally observed in the MFDs of all three types of hierarchical network when arterials are densely distributed as shown in the left and middle column of Fig. 2b, c, and d. By comparison, in the right column of Fig. 2b, c, and d in which arterials are sparsely distributed, the average network flow increases monotonically with density again in the free-flow regime of the MFD.

2.2. *Empirical observations*

Additional evidence of a non-unimodal pattern in a network's MFD is obtained from empirical data in London. The data used for this study came from UTD19 (Loder et al., 2019), a large-scale traffic dataset from over 23,541 stationary detectors on urban roads in 40 cities. The dataset of London contains data measured for 22 days by 4763 loop detectors located on 2046 different roads divided into 5 roadway types: "primary", "secondary", "residential", "tertiary", and "other". To avoid travel behavior inconsistency between workdays and weekends, only the 15 workday data are used in this paper. Data of the Fulham neighborhood in London are used in this paper since it has a clearer hierarchical network structure. Fig. 3a shows the distribution of detectors in London and Fig. 3b shows the network structure of Fulham.

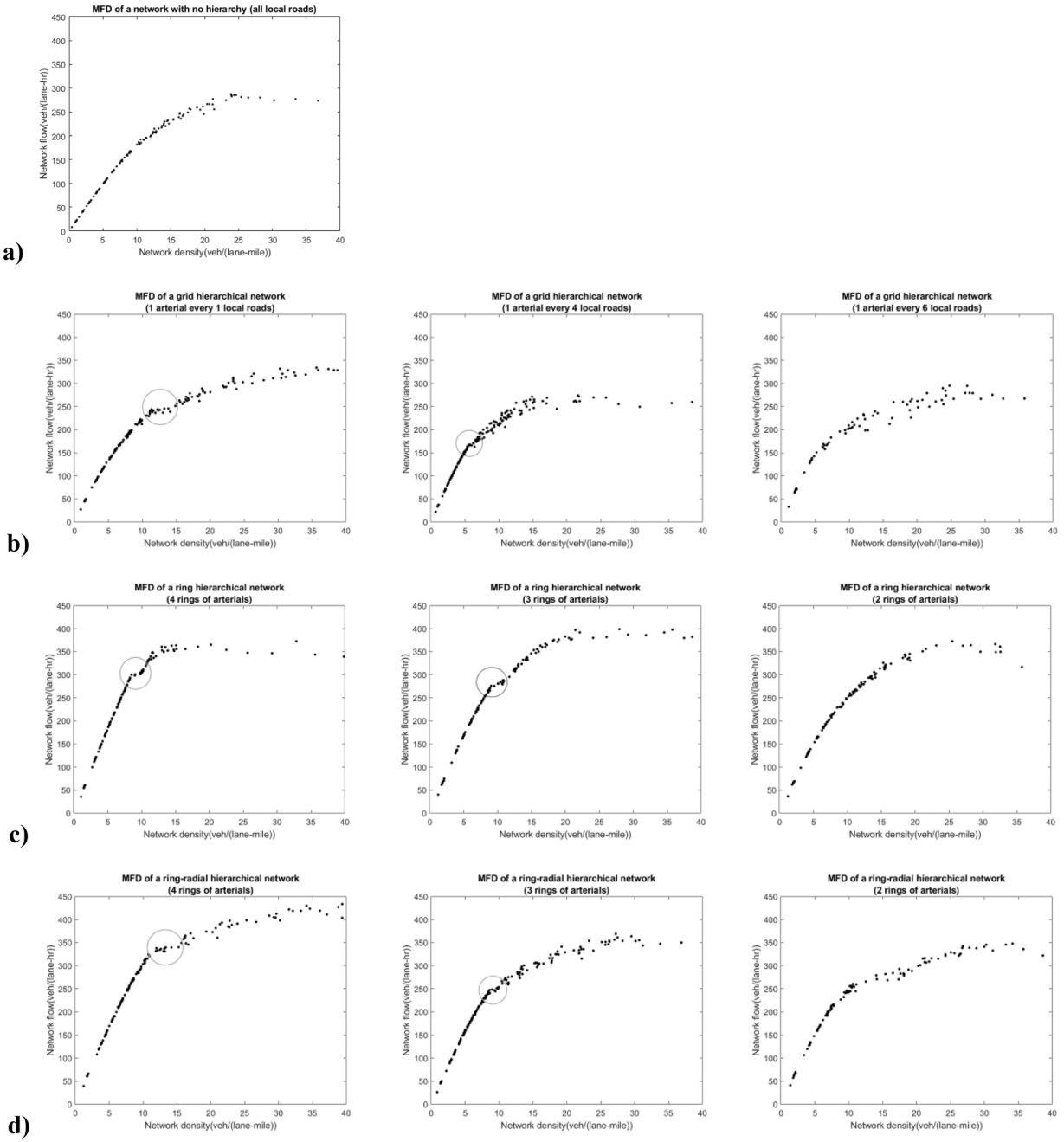

Fig. 2. MFD of) a network with no hierarchy; b) a grid hierarchical network; c) a ring hierarchical network; d) a ring-radial hierarchical network.

The dataset contains flow and occupancy measured by the loop detectors every 5 min. The density is then estimated using occupancy divided by the sum of the average vehicle length and average detector length (Coifman, 2001). This sum is estimated to be 19.69 ft in London (Ambühl et al., 2018).

Due to multiple detectors on the same roads, the flow q_i and density k_i of each road i are obtained by taking the average of flow and density observed by all detectors located on the same road during the same time period. Then the network flow (q_H) and density (k_H) of the entire region during each time period are determined using the generalized definitions of (Edie, 1965) and written as:

$$q_H = \frac{\sum q_i l_i}{\sum l_i} \tag{1a}$$

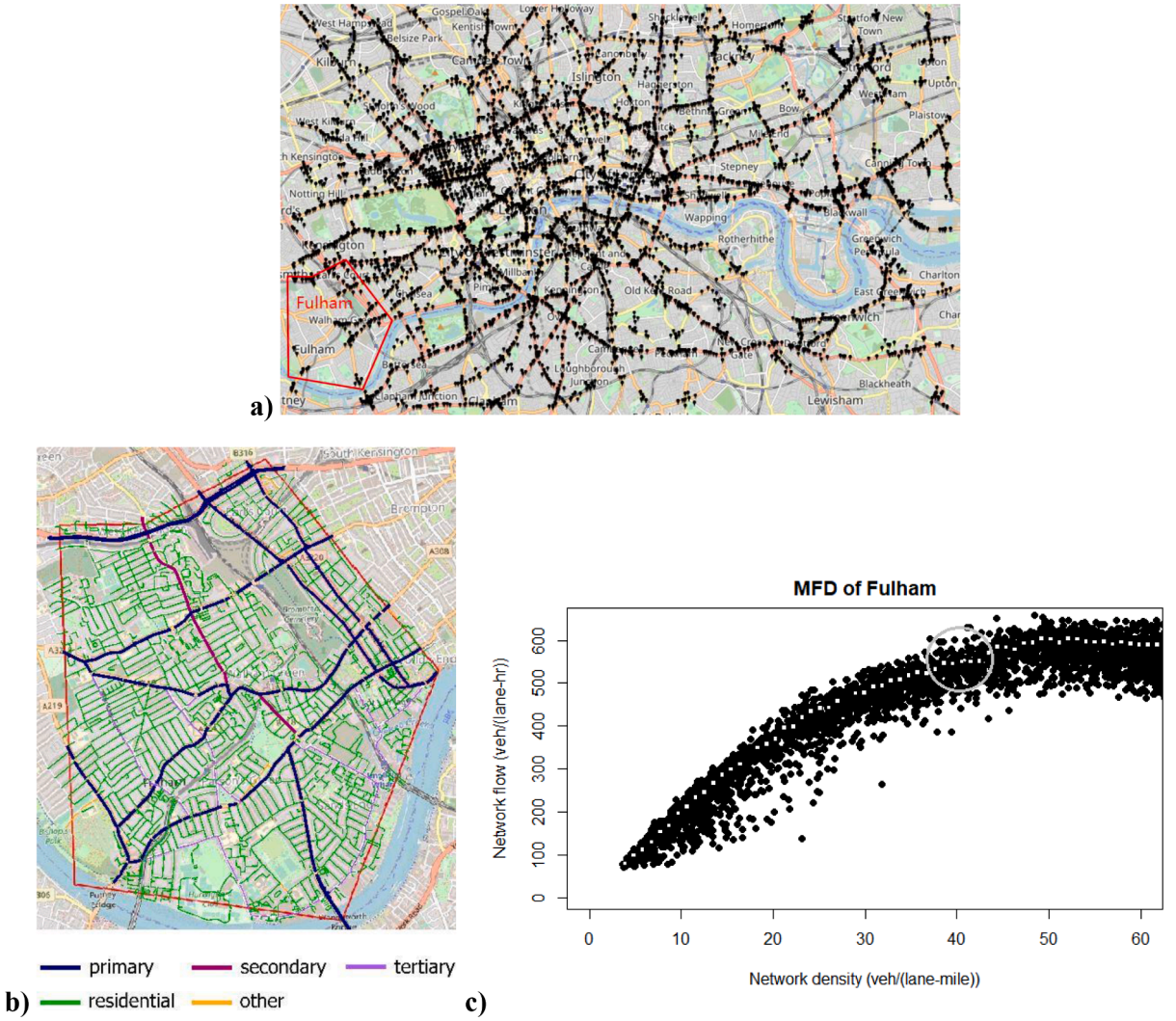

Fig. 3. a) Loop detectors in London; b) Network structure of Fulham; c) MFD of Fulham, London.

$$k_H = \frac{\sum k_i l_i}{\sum l_i} \tag{1b}$$

where l_i is the length of road i.

Finally, as was done in (Ambühl et al., 2019, 2018; Huang et al., 2021; Loder et al., 2019), we divide the flow-density pairs into multiple small density bins with equal lengths of X [veh/(lane-mile)] and use the median of the top Y (in percent) flow values per density bin to fit the upper bound of MFD. The median is used to avoid any bias due to outliers (Ambühl et al., 2018). To balance the need for sufficient data pairs in each density bin and the concern of averaging the real MFD shape, we finally chose X to be 1 veh/(lane-mile) and Y to be 50% after several trials. However, it should be noted that the general conclusion does not change with other values. Fig. 3c shows the resulting MFD of Fulham. A smooth upper bound in white can be observed. The network flow q_H first increases in the range $k_H \in (0, 38)$ veh/(lane-mile), then remains relatively unchanged in the range $k_H \in (38, 43)$ veh/(lane-mile), and finally increases again until the capacity is reached. This non-unimodal pattern is similar to the pattern observed in the AIMSUN simulations.

Possible explanations for this non-concave pattern are explored in the following sections. A simple hierarchical linear corridor is first explored. Then the analytical analysis is extended to a more realistic two-dimensional network.

3. Hierarchical one-way linear corridor with limited access

In this section, we analytically study a simple hierarchical network system to better understand the non-unimodal patterns that arise in MFDs of networks with hierarchical structures. The simple system considered is a one-way linear corridor. Without loss of

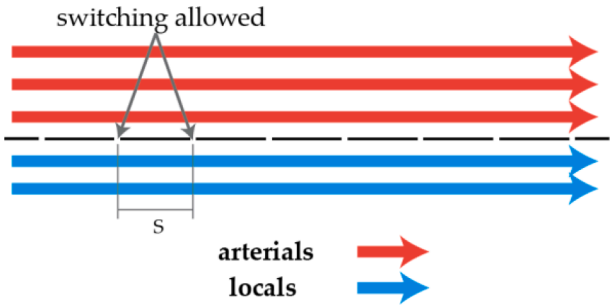

Fig. 4. Graphical depiction of a linear corridor.

Table 1
Average trip distance on each roadway type.

OD pair z	Percentage of OD pairs, $P(z)$	Strategy 1		Strategy 2	
		$D_l^1(z)$	$D_a^1(z)$	$D_l^2(z)$	$D_a^2(z)$
LL	p_l^2	D	0	S	$D-S$
LA	$p_l p_a$	$D-\frac{S}{2}$	$\frac{S}{2}$	$\frac{S}{2}$	$D-\frac{S}{2}$
AL	$p_l p_a$	$D-\frac{S}{2}$	$\frac{S}{2}$	$\frac{S}{2}$	$D-\frac{S}{2}$
AA	p_a^2	$D-S$	S	0	D

generality, we assume two street types are available on this corridor: arterials (a) and local roads (l). A well-defined MFD is assumed to exist for each roadway type $i \in \{a, l\}$ that relates its average flow, q_i, to its average density, k_i. We denote this MFD $Q_i(k)$, where $q_i = Q_i(k_i)$. Note also that the average travel speed on each roadway type i is a function of the density on that roadway type and the MFD, $v_i = V_i(k_i) = Q_i(k_i)/k_i$. If the total length of each roadway type, L_i [lane-mile], is also known, the average flow (q_H) and density (k_H) on the entire corridor system can be determined using the generalized definitions of (Edie, 1965) and written as:

$$q_H = \frac{q_a L_a + q_l L_l}{L_a + L_l} \tag{2a}$$

$$k_H = \frac{k_a L_a + k_l L_l}{L_a + L_l} \tag{2b}$$

We assume that vehicles cannot switch freely between the two roadway types. Instead, vehicles can only travel between the two roadway types at predesignated points located some distance S [mile] apart; see Fig. 4. These switching locations are analogous to intersections in a two-dimensional network where vehicles can turn from one roadway type to another. In a linear corridor, this would represent access points. Such access points exist in several linear transportation facilities, e.g., HOV lanes with limited entry locations.

We also assume that p_l percent of trips begin and end on local roads and that p_a percent of trips begin and end on arterials ($p_l + p_a = 1$). Therefore, there are four types of origin-destination (OD) pairs: both origin and destination on local (LL), origin on local and destination on arterial (LA), origin on arterial and destination on local (AL), and both origin and destination on arterial (AA)

3.1. Analytical method to obtain the system-wide MFD

The MFD of this linear system would depend on how many vehicles use the arterials vs. the local roads, as shown in Eq. (2), which would depend on vehicle routing behavior. To study this further, we assume that each vehicle has two routing options to complete its trip: 1) primarily use local roads (i.e., only use arterials to access the local roads); or, 2) primarily use arterials (i.e., only use local roads to access the arterials). For example, consider the LL OD case. Under strategy 1, vehicles will stay on the local roads for their entire trip, while under strategy 2 vehicles will use the local roads to access the arterial, travel on the arterial to approach their destination, and then use local roads to access their destination.

Let D be the average shortest-path distance between OD pairs ($L_i \gg D$ for any roadway type i). If the spatial distributions of origins and destinations are known, then the average distance traveled per trip on roadway type i under each combination of routing option j ($j = 1$ *or* 2) and OD pair z ($z = LL, LA, AL,$ *or* AA), $D_i^j(z)$, can be estimated using continuum approximation principles, as in (Daganzo, 2010). Table 1 provides these values for all OD pair-routing option combinations and the percentage of each type of OD pair, $P(z)$, assuming that origins and destinations on each roadway type are distributed uniformly in space.

Denote the fraction of vehicles that use strategy 1 by p. The ratio of flow on the arterial and local roads would be related by the total distance traveled on each of the two roadway types according to the generalized definitions of flow (Edie, 1965) as follows:

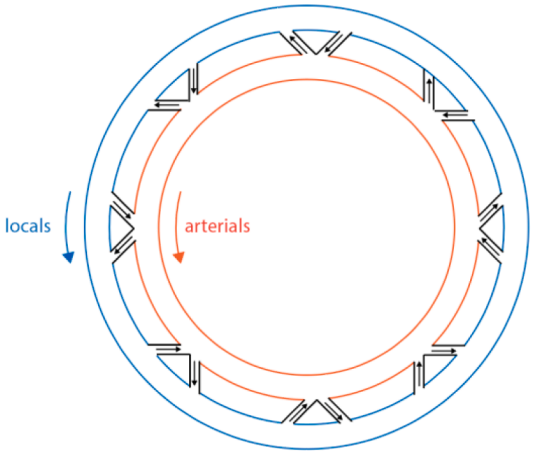

Fig. 5. Simulated hierarchical one-way linear corridor.

$$\frac{q_l}{q_a} = \frac{L_a}{L_l} \times \frac{\left[p \times \sum_z P(z) \times D_l^1(z) + (1-p) \times \sum_z P(z) \times D_l^2(z)\right]}{\left[p \times \sum_z P(z) \times D_a^1(z) + (1-p) \times \sum_z P(z) \times D_a^2(z)\right]}$$
$$= \frac{L_a}{L_l} \times \frac{p \times \left[p_l^2 \times D + 2 \times p_l p_a \times \left(D - \frac{S}{2}\right) + p_a^2 \times (D-S)\right] + (1-p) \times \left[p_l^2 \times S + 2 \times p_l p_a \times \frac{S}{2} + p_a^2 \times 0\right]}{p \times \left[p_l^2 \times 0 + 2 \times p_l p_a \times \frac{S}{2} + p_a^2 \times S\right] + (1-p) \times \left[p_l^2 \times (D-S) + 2 \times p_l p_a \times \left(D - \frac{S}{2}\right) + p_a^2 \times D\right]} \tag{3}$$

For given values of p and average density on the hierarchical system, k_h, the flow and density on each of the local and arterial roads can be obtained by solving the set of equations given by (2b), (3), and the MFD relationships, $q_i = Q_i(k_i)$. The corresponding average flow in the system can then be obtained from (2a). Thus, what is left to be determined is the value of p. The remainder of this section considers two scenarios: 1) vehicles route themselves to minimize their personal travel time (user equilibrium); and, 2) vehicles are routed to minimize the average travel time of all vehicles in the system (system optimal).

3.1.1. User equilibrium (UE) conditions

This section considers the case in which vehicles behave according to Wardrop's first principle (Wardrop, 1952) and route themselves in such a way as to minimize their own travel time. Consider the average travel times using option 1, $tt_1(k_H,p)$, and option 2, $tt_2(k_H,p)$, as a function of average network density k_H and fraction of vehicles using strategy 1 p:

$$tt_1(k_H,p) = \sum_z P_z \times \left(\frac{D_l^1(z)}{V_l(k_l)} + \frac{D_a^1(z)}{V_a(k_a)}\right) = p_l^2 \times \frac{D}{V_l(k_l)} + 2 \times p_l p_a \times \left(\frac{D - S/2}{V_l(k_l)} + \frac{S/2}{V_a(k_a)}\right) + p_a^2 \times \left(\frac{D-S}{V_l(k_l)} + \frac{S}{V_a(k_a)}\right) \tag{4a}$$

$$tt_2(k_H,p) = \sum_z P_z \times \left(\frac{D_l^2(z)}{V_l(k_l)} + \frac{D_a^2(z)}{V_a(k_a)}\right) = p_l^2 \times \left(\frac{S}{V_l(k_l)} + \frac{D-S}{V_a(k_a)}\right) + 2 \times p_l p_a \times \left(\frac{S/2}{V_l(k_l)} + \frac{D - S/2}{V_a(k_a)}\right) + p_a^2 \times \frac{D}{V_a(k_a)} \tag{4b}$$

The optimal routing strategy under UE conditions for any k_h would be that which provides travel times such that no vehicles can reduce their travel times by changing routing options. This can be found in the following optimization problem:

$$\min_p \int_o^p tt_1(k_H,p)dp + \int_o^{1-p} tt_2(k_H,p)dp \tag{5}$$

which is subject to (2b), (3), the MFD relationships, and non-negativity constraints. Note that these equations assume that p is the same for each type of OD pair. This can be easily relaxed in Eq. (3); however, doing so does not significantly change the final MFD estimation while increasing the complexity of the formulation and analytical solution. Moreover, in all cases tested numerically, MFD assuming that p is the same for each type of OD pair matches well with MFD assuming that p is different for each type of OD pair. Thus, this assumption is maintained for simplicity.

3.1.2. System optimal (SO) conditions

Under Wardrop's second principle (Wardrop, 1952), vehicles select between the competing options to minimize the average travel time of all vehicles, $\bar{tt}$, in the network. In this case, the solution is found using the following optimization problem:

$$\min_p \bar{tt}(p) = \min_p p \times tt_1(p) + (1-p) \times tt_2(p) \tag{6}$$

If holding the average density within the network fixed and minimizing the average travel time for each vehicle (maximizing the average speed), the average flow within the network would thus be maximized. Thus, this condition maximizes the average flow (q_H)

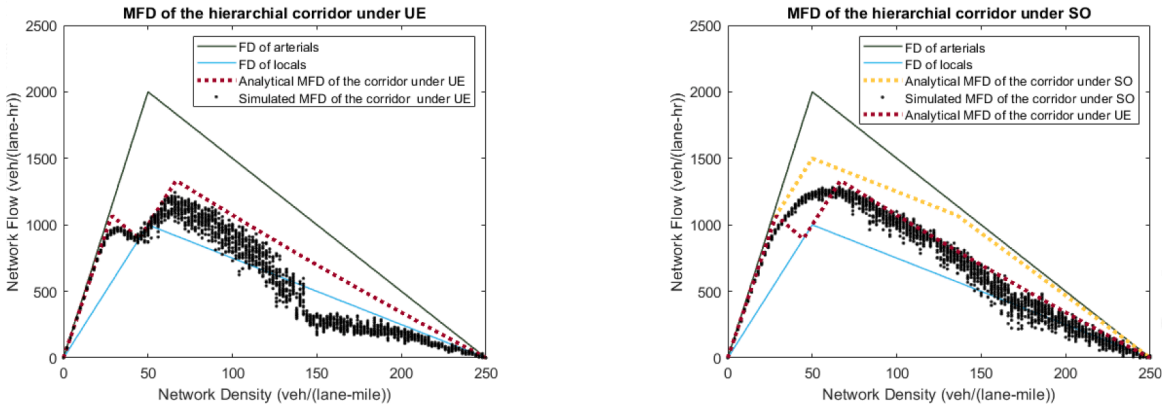

a) MFDs

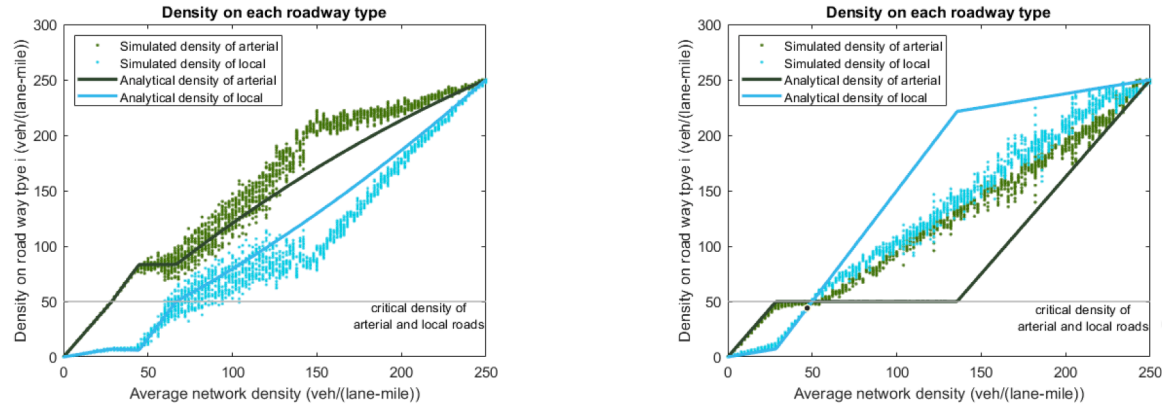

b) Densities on individual roadway types

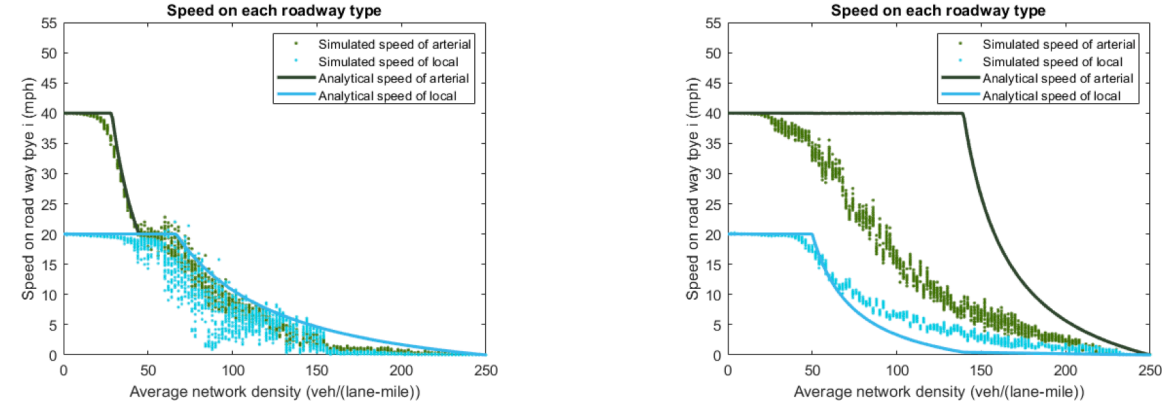

c) Speeds on individual roadway types.

Fig. 6. Comparison of UE and SO.

in the system for a given average system density.

3.2. Simulation verification

A simulation of an infinite arterial corridor (i.e., ring road) is used to validate the MFDs obtained from the analytical derivations.

This section describes the simulation parameters and compares the results with the analytical model.

3.2.1. Simulation description

In this section, a dual ring network is simulated to study the MFD of a hierarchical one-way corridor. The network simulated here—shown in Fig. 5—consists of two one-way streets arranged to form concentric rings. One ring represents the arterial streets while the other the locals. The arterial street is assumed to have one travel lane on which traffic obeys a triangular fundamental diagram with a free flow speed (40 mile/hr), capacity (2000 veh/(lane-hr)), and jam density (250 veh/(lane-mile)). Each local street also has one travel lane on which traffic obeys a triangular fundamental diagram with a common free flow speed (20 mile/hr), capacity (1000 veh/(lane-hr)) and jam density (250 veh/(lane-mile)). Vehicles can only travel between the two roadway types at predesignated points located every 0.5 mile.

Vehicles on the network were simulated using the cellular automata model (CAM) proposed by (Daganzo, 2006), which is consistent with kinematic wave theory (Lighthill and Whitham, 1955a, 1955b; Richards, 1956). In this framework, each street is broken up into homogeneous discrete cells of length 0.004 miles (equal to average vehicle spacing at jam density), which allows only a single vehicle to occupy any cell at any time period. Vehicle locations on arterials are updated at consistent intervals of 0.36 s while vehicle locations on local roads are updated at consistent intervals of 0.72 s. Average flow and density across the entire network are computed using the generalized definitions proposed by (Edie, 1965) at discrete intervals of 6 min.

The simulation starts with an empty network. Vehicles gradually enter the network with their origins and destinations uniformly distributed across all arterial and local streets until the average density of the network reaches a predefined value. This density is then maintained for the length of the simulation run. To do this, vehicles that arrive at their destinations are immediately replaced by a randomly generated new trip. It is also assumed that entering vehicles have priority over vehicles in the network. In the results shown here, the distance traveled for an individual trip is drawn randomly from a uniform distribution between 2.4 miles to 3.6 miles.

Under UE routing, each vehicle chooses its travel strategy based on the estimated travel time calculated using the average speed of local roads and arterials of the last 1-minute period by the time it enters the network. SO routing is more complex and is only estimated in the simulation. Under the SO routing, multiple simulations are performed with the density of arterials held constant around some different pre-determined values by controlling the number of vehicles that uses strategy 2. The simulation with the pre-determined arterial density that maximizes the average network flow is then used to obtain the MFD under SO.

3.2.2. Results under UE routing

The left side of Fig. 6a illustrates the fundamental diagrams for local and arterial roads, as well as the analytically derived MFD for the corridor and observed flow-density relationship in the simulation under UE routing conditions. As expected, the UE MFDs fall somewhere between the individual fundamental diagrams of the local roads and arterials. The network-wide flow-density relationships obtained analytically and from the simulation are remarkably consistent, particularly in the uncongested and capacity regimes. Small differences between the simulated and analytical MFDs occur when the network is highly congested. This is likely due to the tendency of ring networks to become imbalanced and gridlocked when heavily congested (Daganzo et al., 2011; Gayah et al., 2014).

Notice that the network-wide MFD is not unimodal or concave under UE routing conditions. On the left side of Fig. 6a, flow increases with density in the range $k_H \in (0, 28)$ veh/(lane-mile), decreases in the range $k_H \in (28, 44)$ veh/(lane-mile), increases again in the range $k_H \in (44, 67)$ veh/(lane-mile), and finally decreases from $k_H \in (67, 250)$ veh/(lane-mile). Fig. 6b plots the density on each individual roadway type as a function of the average density. Considering Fig. 6a and b together, we can observe that the latter decreasing section of MFD in the range $k_H \in (67, 250)$ veh/(lane-mile) on the left side of Fig. 6a represents the congested branch in which both the local and arterial roads are congested as densities of both arterial and local road exceed density at capacity for $k_H \in (67, 250)$ veh/(lane-mile) on the left side of Fig. 6b. By contrast, the former decreasing section of MFD in the range $k_H \in (0, 28)$ on the left side of Fig. 6a represents cases in which the arterial is congested but local roads are not as the density of arterial exceeds density at capacity while the density of local roads is far from density at capacity for $k_H \in (0, 28)$ veh/(lane-mile) on the left side of Fig. 6b. Examination of Fig. 6c, which plots the speed on each individual roadway type as a function of the average density, confirms this. The first decreasing section of the MFD corresponds to a situation where the arterial speed decreases with increased density, but is still larger than the speed of traveling on the arterials. Consequently, the arterials are used more than the locals. However, eventually, speeds on the arterials and locals become similar and remain constant with increasing density. This is associated with increased use of the local roads—and thus increasing flows in the MFD. Finally, speeds on both the arterials and local roads both decline with density, which is associated with the congested branch of the MFD. The result is the non-concave MFD pattern in the free flow regime. Repeated tests show that this non-unimodal and non-concave shape is a general finding under various scenarios and settings in both the simulation environment and analytical derivation under UE routing conditions.

3.2.3. Results under SO routing

The right side of Fig. 6a provides the fundamental diagrams for the local and arterial roads, as well as MFDs obtained analytically and from the simulation under SO routing conditions, while the right side of Fig. 6b provides the density on each individual roadway type as a function of the average network density for this case. Great consistency is observed between the analytically obtained and simulated flow-density relationship in the uncongested and near-capacity regimes. However, the simulation results show that the network becomes unstable when it starts to get congested. Differences between the analytically derived MFD and the MFD observed in the simulations tend to grow as the network becomes more congested. Several reasons account for this discrepancy problem:

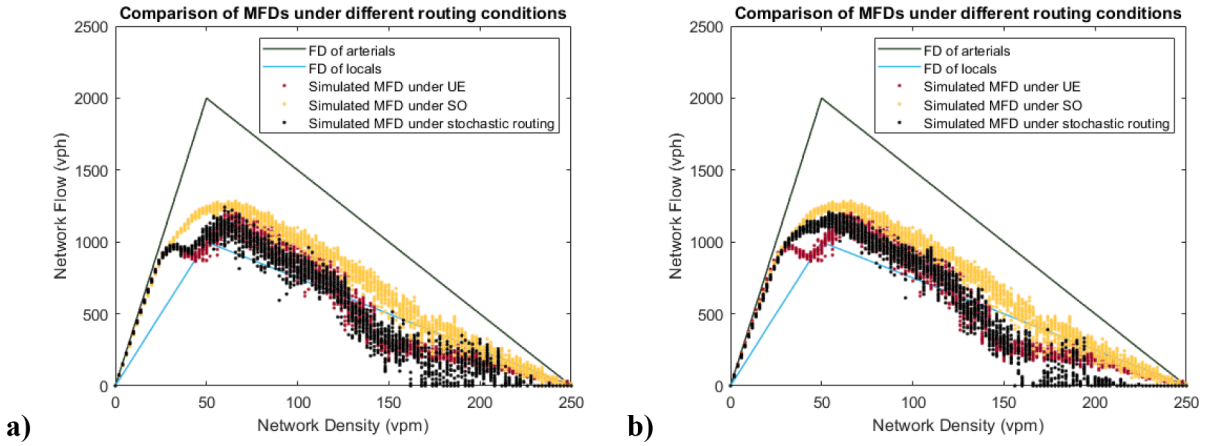

Fig. 7. Comparison of MFDs under different routing conditions when a) $\beta = 2.5$ and b) $\beta = 0.5$.

1 As in the UE case, the network has the tendency towards inhomogeneous congestion distributions and will produce non-MFD states as it gets congested and unstable, as identified in many previous works (Daganzo et al., 2011; Gayah et al., 2014; Mazloumian et al., 2010; Saberi et al., 2014).
2 Constraint (3) which provides the relationship between flows of the two roadway types is only valid in a long stable period where all vehicles should be able to finish their trips. However, in the simulations, when the network gets so congested that many vehicles cannot finish their trip in the simulated period, the flow relationship will not be the same as the analytical solution suggested.
3 Bottlenecks arise at the transition points between locals and arterials. The analytical solution suggests that the arterial should be always used with the flow as high as possible, which makes the local roads have a high density and a low flow when the network is congested. The significant discrepancy between flows of the two roadway types makes it extremely difficult for vehicles to turn from arterials to the local roads in the linear corridor. As a result, bottlenecks may form at the transition points, which makes the network highly unstable.

Differences between UE and SO in Fig. 6b and c indicate that vehicles tend to use arterials more than locals to minimize their own travel time under UE conditions. As a result, the speed of arterials has already dropped dramatically at a low network density. By contrast, arterials are used at their capacity under the SO condition, which provides a higher overall flow, a faster average travel speed and a shorter travel time to all vehicles in the network. This suggests that hierarchical networks can be made more productive by carefully routing vehicles within the network. Comparisons of the UE and SO MFDs in Fig. 6a also show that the MFDs are unimodal and concave in the SO, whereas they are not in the UE case.

3.2.4. *Results under stochastic routing*

In addition to user equilibrium (UE) and system optimal (SO) conditions, a stochastic routing condition is also simulated for comparison. Under stochastic routing conditions, the probability of each vehicle using routing option 1 is expressed by a logistic (logit) model using real-time variables. Specifically, the probability of a vehicle using option 1 determined by the time it enters the network, p_{s1}, is given by:

$$p_{s1} = \frac{1}{1 + \exp(-\beta[tt_2 - tt_1])}. \tag{7a}$$

where tt_1 is the predicted travel time of a vehicle using option 1 and tt_2 is the predicted travel time of a vehicle using option 2 estimated by the real-time speeds on each arterial and local street. β is a scaling factor that reflects people's value of time. The corresponding probability of using option 2, p_{s2}, is:

$$p_{s2} = \frac{1}{1 + \exp(-\beta[tt_1 - tt_2])} \tag{7b}$$

Two different scaling factors, 0.5 and 2.5, are used for the simulations under stochastic routing condition. Fig. 7a and b provide comparisons of network MFDs obtained from the simulations under the UE routing conditions, the SO routing conditions, and the stochastic routing conditions. In both figures, MFD under stochastic routing conditions lies somewhere between MFD under UE condition and MFD under SO condition. When β is large, small differences in travel time between the two routing options are weighted heavily, and this causes travelers to become more likely to use the shortest-travel time route. As a result, the MFD under stochastic turning shows a non-unimodal pattern and is closer to MFD under UE condition than MFD under SO condition, shown in Fig. 7a. By contrast, when β is small, travelers are relatively insensitive to small differences in travel times between the two routing options, which causes travelers to more evenly distribute themselves between the competing routes. The resulting MFD under stochastic turning does not display a non-unimodal pattern and is closer to MFD under SO condition than MFD under UE condition, shown in Fig. 7b.

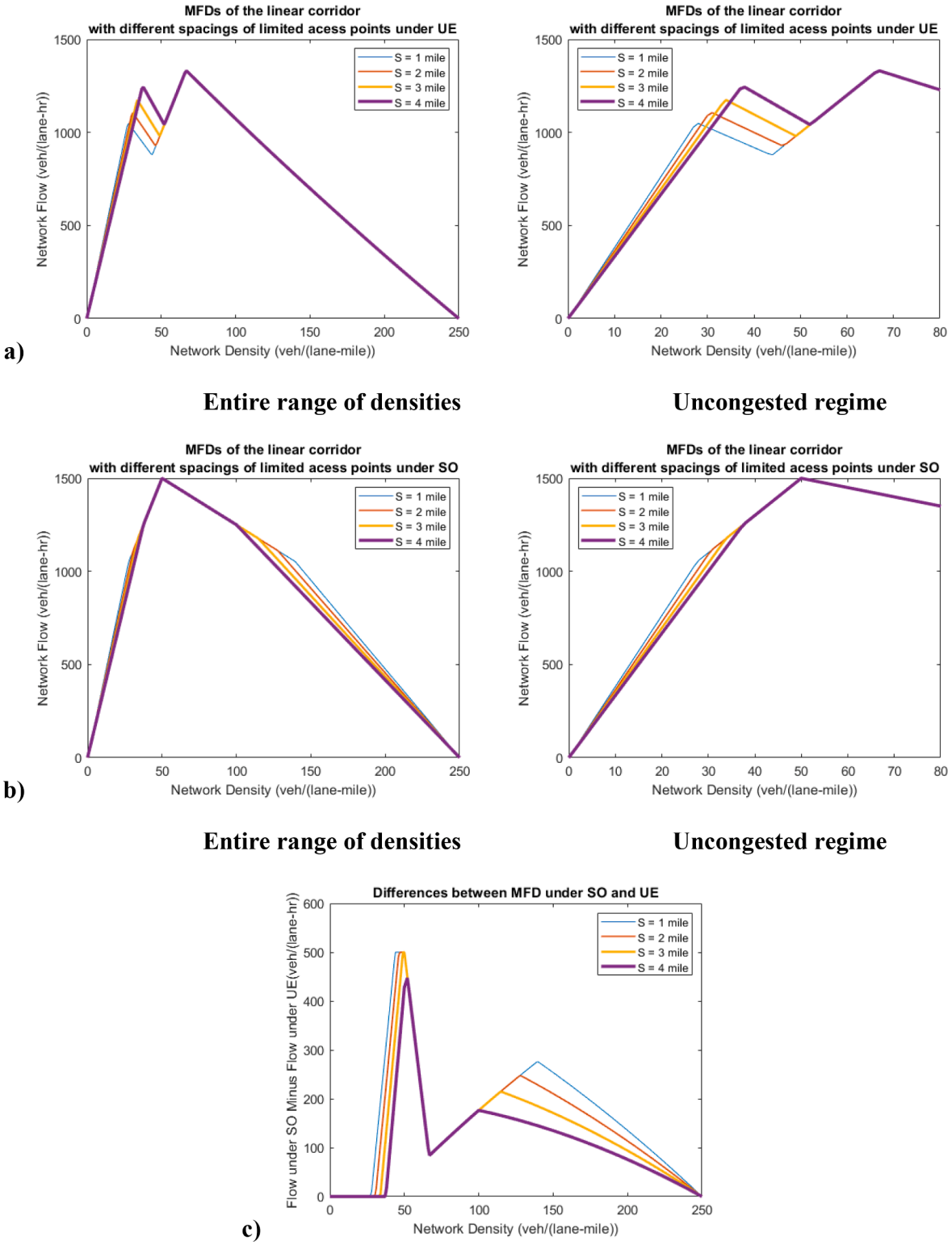

Fig. 8. a) Comparison of MFDs for linear corridors with different spacings of transition points under UE conditions; b) Comparison of MFDs for linear corridors with different spacings of transition points under SO conditions; and, c) Differences between MFD under SO condition and MFD under UE condition.

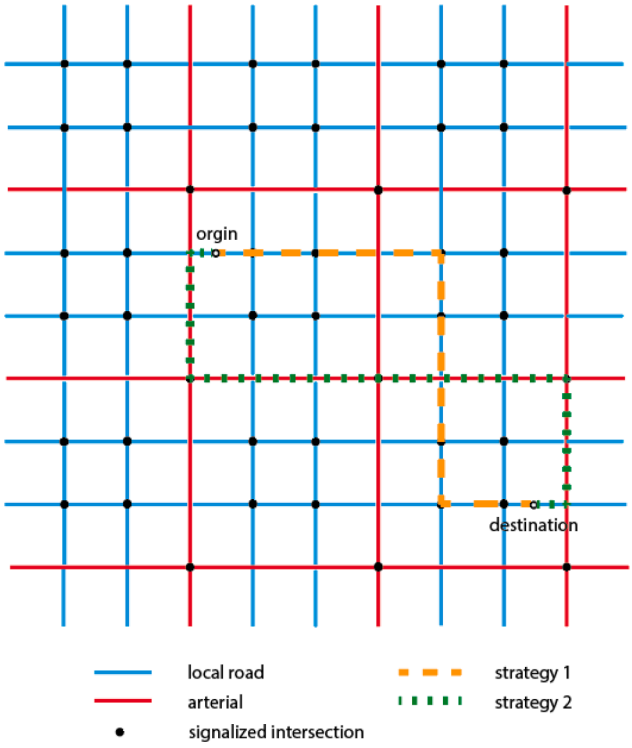

Fig. 9. Two-dimensional hierarchical network.

Comparison of Fig. 7a and b shows that when more people are 'selfish' and are trying to minimize their own travel time, the efficiency of the network in terms of flow will be compromised.

3.3. Sensitivity of S

The following numerical example illustrates how the spacing of transition points can affect the MFD of a one-way linear corridor. Fig. 8a and b illustrate the MFDs of the entire hierarchical system with different spacings under UE and SO routing assumptions, respectively, assuming the same FD for the local and arterial networks as in the previous section. Under UE routing conditions, smaller transition spacings lead to higher flows at low network densities. However, larger transition spacings have a higher first apex of the MFD. The rest of the MFD is insensitive to this spacing. Since maximizing network flow at or near these peaks is most critical to accommodate surges in demand, a larger transition spacing would be preferred under UE routing conditions. By contrast, smaller transition spacings lead to higher network flow for most part of the uncongested regime and congested regime under SO conditions.

Fig. 8c shows the difference in average flows observed for each density under the SO and UE conditions. This is related to the price of anarchy or the loss in network efficiency that occurs by allowing travelers free will to make routing decisions. As expected, this difference is greater than or equal to zero for all spacing values, since the SO MFD is always greater than or equal to the UE MFD. In general, the difference between the SO and UE flows decreases with the transition spacing. This occurs because vehicles have to travel longer distances before switching between roadway types as the transition spacing increases, and this results in the decision variable p having a reduced impact on the network MFD. Therefore, even if different p values are obtained for the UE and SO cases, the resulting MFDs will be close.

By understanding how these two routing assumptions impact the MFD, agencies can design the network based on their objectives and how much flexibility travelers have in routing. If agencies care about user equilibrium allowing people to choose their paths that minimize their own travel time, then a smaller spacing is preferred. If agencies seek to minimize the difference between observed network efficiency and maximum network efficiency (i.e., the price of anarchy) or have limited ability to induce certain routing behaviors, a larger spacing is preferred as it results in smaller differences between MFDs of the two routing conditions.

4. Hierarchical two-dimensional network

Now, we extend the analytical formulations to examine how hierarchical structures might influence the MFD of two-dimensional network structures. Again, without loss of generality, we assume this system is composed of two street types that allow travel in two directions: arterials with N_a travel lanes in each direction, block length (l_a) and total length (L_a), and local roads with N_l travel lanes in each direction, block length (l_l) and total length (L_l). The arterials and locals are assumed to be arranged in a sequence such that there is

Table 2
Average trip distance on each roadway type.

OD pair z	Percentage of OD pairs, P(z)	Strategy 1 $D_l^1(z)$	$D_a^1(z)$	Strategy 2 $D_l^2(z)$	$D_a^2(z)$
LL	$\frac{r^2}{(r+1)^2}$	D	0	$\frac{l_a}{3}$	$D-\frac{l_a}{48}$
LA	$\frac{r}{(r+1)^2}$	D	$\frac{l_l}{4}$	$\frac{l_a}{6}$	D
AL	$\frac{r}{(r+1)^2}$	D	$\frac{l_l}{4}$	$\frac{l_a}{6}$	D
AA	$\frac{1}{(r+1)^2}$	D	$\frac{l_l}{2}$	0	D

one arterial for every $N \in Z+$ locals. An example for $N=2$ is illustrated in Fig. 9. One can easily prove the following two relationships:

$$l_a = (N+1) \times l_l \tag{8a}$$

$$r = \frac{L_l}{L_a} = \frac{N \times N_l}{N_a} \tag{8b}$$

where r refers to the ratio of the total length of local roads to the total length of arterials.

Again, vehicles cannot travel between the two roadway types freely. Instead, vehicles are only able to switch the two roadway types at the intersections of local roads and arterials. Intersections between arterials and intersections between local roads are assumed to be signalized, while intersections involving an arterial and a local road are assumed to be stop-controlled on the minor approach. Moreover, we assume that all trips begin and end on the local roads.

The average flow (q_H) and density (k_H) of this system two-dimensional network can be determined using (2a) and (2b), respectively. As in the linear corridor, we assume that each vehicle has two travel options: 1) mainly use local roads for their trip and only use arterials to access the nearest local road or approach their destination; or, 2) mainly use arterials for their trip and only use local roads to access the nearest arterial or approach their destination. The difference when these strategies are applied in the two-dimensional network is that a vehicle may experience additional total travel distance in order to access the nearest local road or arterial depending on its OD location. For example, Fig. 9 shows the two travel strategies for one combination of OD pair. We can see that when using strategy 1, local roads are used for the entire trip and thus there is no additional trip distance. When using strategy 2, in order to access the nearest arterial from the origin, the vehicle travels additional distance to access the arterial streets.

Table 2 shows the percentage of each OD pair $P(z)$ and the average distance traveled per trip on roadway type i under each OD pair-routing option combination, $D_i^j(z)$, assuming ODs are uniformly distributed across the network. An example derivation of $D_i^j(z)$ for the OD pair LL under routing option 2 is provided in Appendix A.

Let p denote the fraction of vehicles that use routing strategy 1. The ratio of flow on the arterial and local roads would be related by the total distance traveled on each of the two roadway types can be defined similarly to (3) as follows:

$$\frac{q_l}{q_a} = \frac{L_a}{L_l} \times \frac{p \times D + (1-p) \times \left[\frac{r^2}{(r+1)^2} \times \frac{l_a}{3} + \frac{2r}{(r+1)^2} \times \frac{l_a}{6} + \frac{1}{(r+1)^2} \times 0\right]}{p \times \left[\frac{r^2}{(r+1)^2} \times 0 + \frac{2r}{(r+1)^2} \times \frac{l_l}{4} + \frac{1}{(r+1)^2} \times \frac{l_l}{2}\right] + (1-p) \times \left[\frac{r^2}{(r+1)^2} \times \left(D - \frac{l_a}{48}\right) + \frac{2r}{(r+1)^2} \times D + \frac{1}{(r+1)^2} \times D\right]} \tag{9}$$

The remainder of this section describes how MFD of the hierarchical two-dimensional network can be determined under UE and SO conditions.

4.1. Analytical method to obtain the system-wide MFD

4.1.1. UE conditions

Under these assumptions, the corresponding average travel times of using option 1 and option 2, respectively, are:

$$tt_1(k_H, p) = \frac{r^2}{(r+1)^2} \times \frac{D}{V_l(k_l)} + \frac{2r}{(r+1)^2} \times \left(\frac{D}{V_l(k_l)} + \frac{\frac{l_l}{4}}{V_a(k_a)}\right) + \frac{1}{(r+1)^2} \times \left(\frac{D}{V_l(k_l)} + \frac{\frac{l_l}{2}}{V_a(k_a)}\right) \tag{10a}$$

$$tt_2(k_H, p) = \frac{r^2}{(r+1)^2} \times \left(\frac{\frac{l_a}{3}}{V_l(k_l)} + \frac{D - \frac{l_a}{48}}{V_a(k_a)}\right) + \frac{2r}{(r+1)^2} \times \left(\frac{\frac{l_a}{6}}{V_l(k_l)} + \frac{D}{V_a(k_a)}\right) + \frac{1}{(r+1)^2} \times \frac{D}{V_a(k_a)} \tag{10b}$$

Under Wardrop's first principle, the optimal routing strategy for any k_h can be obtained by solving (5), which is subject to constraints (2b), (7), and the MFD relationships and non-negativity constraints. Again, the underlying assumption is that the value of p is the same for all OD pair types. This assumption can be easily relaxed but does not change the final MFD estimations in a significant

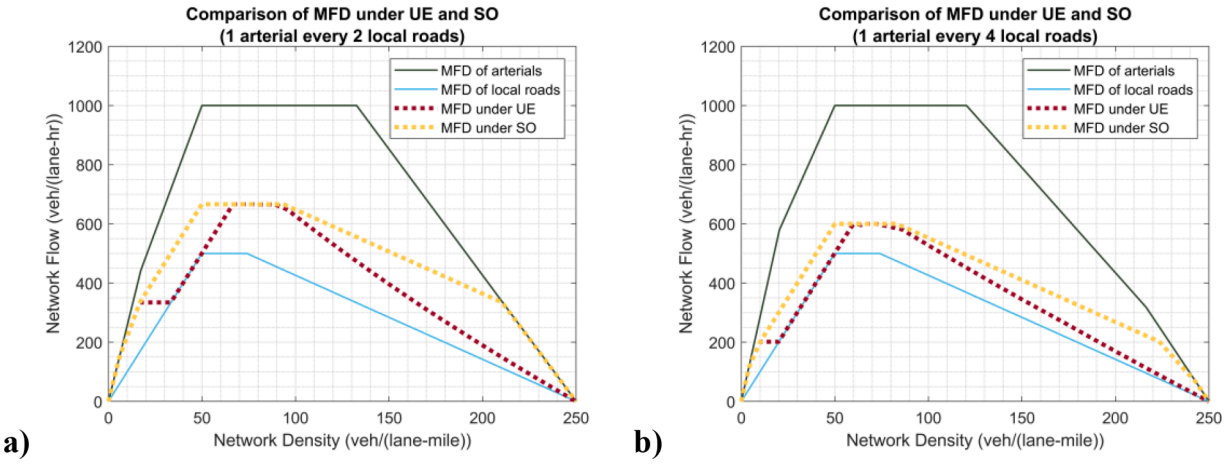

Fig. 10. a) Comparison of theoretical MFD for hierarchical network under UE and SO conditions when the number of local roads are 2 times the number of arterials; b) Comparison of theoretical MFD for hierarchical network under UE and SO conditions when the number of local roads are 4 times the number of arterials.

way.

4.1.2. SO conditions

Under Wardrop's second principle of system optimality, the optimal routing strategy is found by solving (6) which is subject to the same constraints as the UE case.

Note that for a two-dimensional network, this condition is no longer necessarily equivalent to the condition required to maximize the average flow (q_H) in the system for a given average system density. This occurs because the average travel distance changes based on how vehicles route themselves. However, if $D \gg l_l$ and $D \gg l_a$, the additional trip distance arising from switching roadway types is negligible compared to D and the two conditions can be considered equivalent.

4.2. Numerical example

In this section, some key features of MFDs for hierarchical two-dimensional networks are unveiled using a numerical example. Here we consider a grid network composed of arterials and local roads with the same geometry, but different block lengths and fundamental diagrams as shown in Fig. 9. The local roads are assumed to have a block length of 300 ft, a free flow speed of 20 mile/hr, capacity of 1000 veh/(lane-hr) and jam density of 250 veh/(lane-mile). The arterial roads have a free flow speed of 40 mile/hr, capacity of 2000 veh/(lane-hr) and jam density of 250 veh/(lane-mile). The length of arterials depends on N and is given by Eq. (8a). Finally, it is assumed that all local roads and all arterials have one travel lane in each direction. The MFD of both local roads and arterial roads are obtained using analytical methods based on variational theory (Daganzo and Geroliminis, 2008) as a function of block length, signal settings, and fundamental diagram of individual links. Assume all signals have exactly the same green period equal to half of the cycle length of 72 s. Moreover, vehicles are assumed to travel an average distance of $D = 10$ mile.

Fig. 10a and b illustrate the MFDs for the local and arterial roads, as well as the MFD of the entire hierarchical network under both the UE and SO optimal routing assumptions. The MFDs are estimated for the cases when the number of local roads is 2 times and 4 times the number of arterials, respectively. From (8a), we can obtain that the corresponding block lengths of arterials are 900 ft ($N = 2$) and 1500 ft ($N = 4$), respectively.

As expected, the network MFDs always fall somewhere between the individual MFDs of the local and arterial roadways and the MFD under SO routing always has higher flows for a given density than the MFD under UE routing conditions. Again, the MFD under UE routing conditions is not concave, but is unimodal. In Fig. 10a, the network flow under UE first increases with network density in the range $k_H \in (0, 17)$ veh/(lane-mile) and then remains constant in the range $k_H \in (17, 33)$ veh/(lane-mile). This flat section corresponds to the condition when arterials have reached capacity while local roads are still in free flow. Different from the former decreasing section in the MFD of the hierarchical corridor, the MFD of the hierarchical grid network under UE remains constant when arterials reach capacity. This is because arterials immediately become congested after reaching to capacity in the hierarchical corridor while arterials remain at capacity for some densities in the grid network. Then, the network flow increases with the network density again in the range $k_H \in (33, 67)$ veh/(lane-mile) until both arterials and local roads reach to capacity. Finally, the network flow decreases with the network density in the range $k_H \in (89, 250)$ veh/(lane-mile) as arterials and local roads are both congested. Similar patterns can also be observed in Fig. 10b.

Moreover, by comparing Fig. 10a and b, it is clear that the ratio of the number of local roads to the number of arterials (N) not only has a great impact on the shape of MFD of arterials, but affects the shape and capacity of MFD of the hierarchical network as well. A smaller N indicates a denser arterial network, which leads to higher network flow and overall capacity under both UE and SO routing

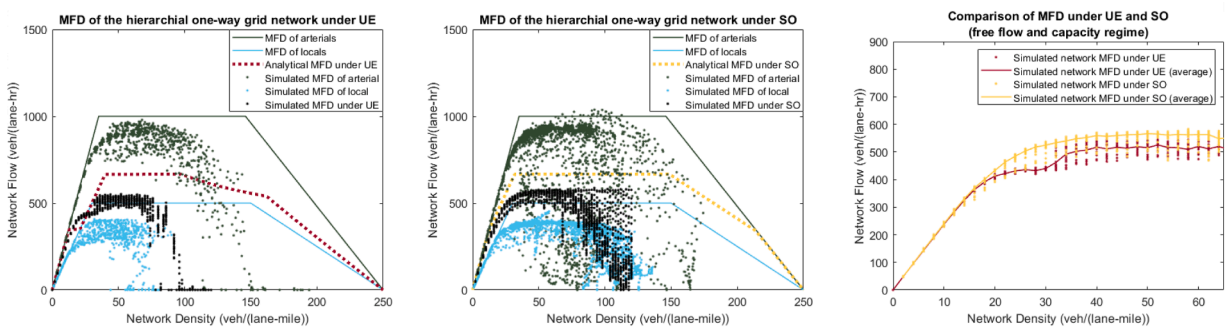

a) MFDs

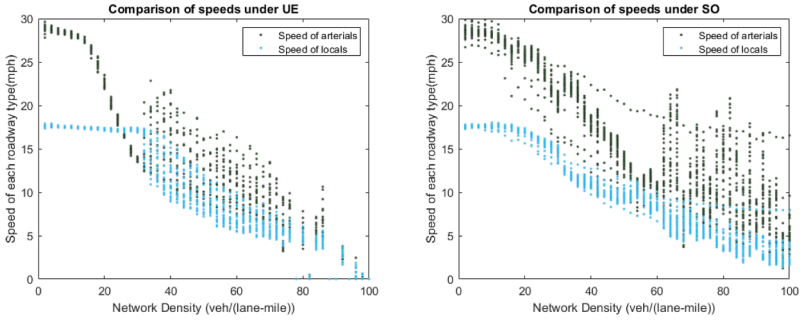

b) Speeds on individual roadway types.

Fig. 11. Comparison of simulation results under UE and SO.

conditions. Note that if the arterial network is too dense (the block length of arterials is too short), the capacity of arterials will be significantly reduced due to queue spillovers.

4.3. Simulation verification

A simulation of a one-way grid network is used to validate the MFDs obtained from the analytical derivations. The network simulated here consists of one-way streets (for simulation simplicity) arranged into a simple 9×9 square grid pattern shown in Fig. 1. The two types of roads are arranged such that for every 2 local roads, there is 1 arterial. The arterial street is assumed to have one travel lane on which traffic obeys a triangular fundamental diagram with a free flow speed (40 mile/hr), capacity (2000 veh/(lane-hr)), and jam density (250 veh/(lane-mile)). Each local street also has one travel lane on which traffic obeys a triangular fundamental diagram with a common free flow speed (20 mile/hr), capacity (1000 veh/(lane-hr)), and jam density (250 veh/(lane-mile)).

The same parameters as the previous section are applied to the cellular automata model (Daganzo, 2006), which is used to simulate the vehicles on the network. In this simulation, vehicle locations on arterials are updated at consistent intervals of 0.36 s while vehicle locations on local roads are updated at consistent intervals of 0.72 s. Note that unlike vehicles in the real world, vehicles on the minor approach of the stop-controlled intersection in the simulation cannot wisely utilize the gap of vehicles on the major approach and thus can possibly be trapped at the intersection for an unreasonably long time. Therefore, all intersections are assumed to be signalized in our simulations to avoid a significant reduction of capacity of local roads. A signal that has a cycle length of 72 s is used at all intersections with an equal green time of 36 s provided to both competing directions. The signal offsets are set to be 0.

The simulation starts with an empty network. Vehicles gradually enter the network with their origins and destinations uniformly distributed across all arterial and local streets until the average density of the network reaches a predefined value. To maintain a constant density throughout the simulation, periodic boundary conditions are maintained in which vehicles exiting the network at the downstream-most point of a given street are reinserted at the upstream-most point of that street. Moreover, vehicles that arrive at their destinations are immediately replaced by a randomly generated new trip. In the results shown here, the distance traveled for an individual trip is drawn randomly from a uniform distribution between 4 miles to 6 miles.

To approximate UE routing conditions, each vehicle chooses its travel strategy based on the estimated travel time calculated using the average speed of local roads and arterials of the last 1-minute period by the time it enters the network. To approximate SO routing conditions, multiple simulations are run with different pre-determined percentages of vehicles that use strategy 1. The simulation with the pre-determined percentage of vehicles using strategy 1 that maximizes the average network flow is then used to obtain the MFD under SO routing.

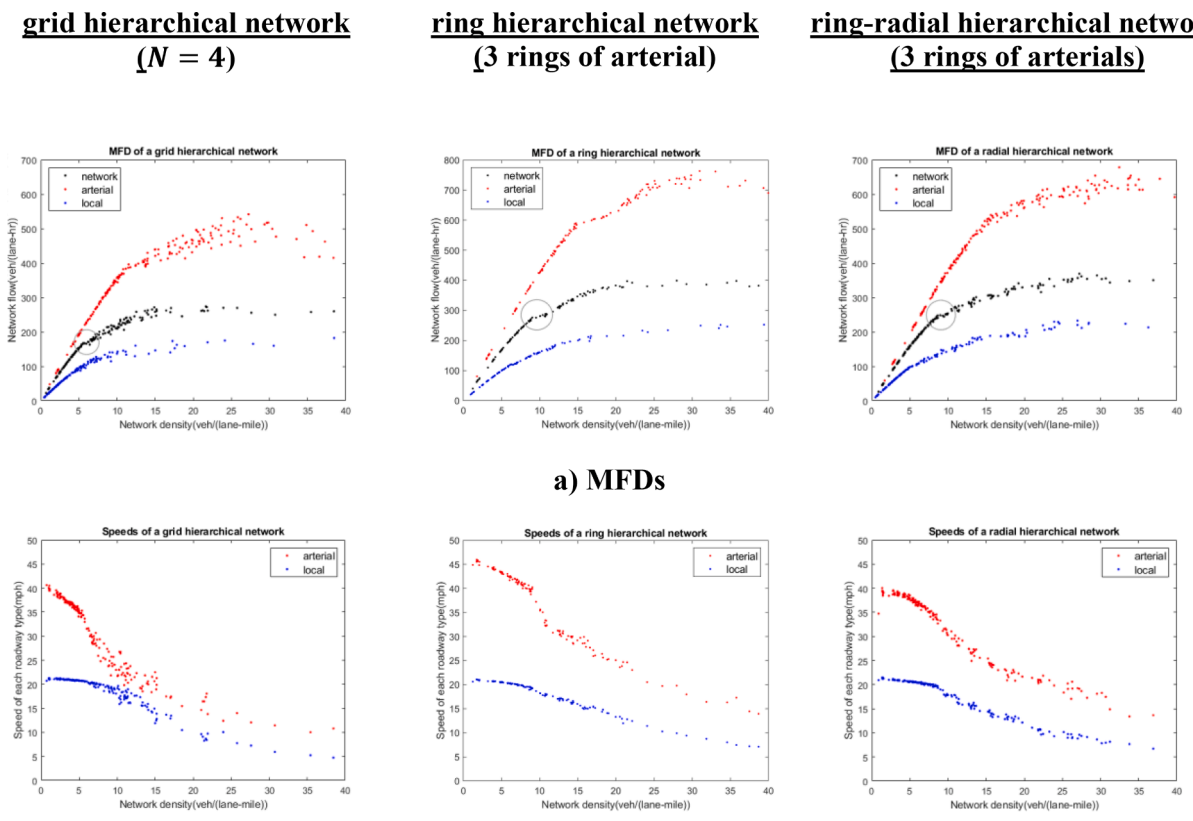

Fig. 12. Validation of AIMSUN results.

The left side of Fig. 11a shows the MFDs of arterial roads, local roads, and the hierarchical network from the simulation under UE routing conditions, while the middle of Fig. 11a shows the MFDs of arterial roads, local roads, and the hierarchical network from the simulation under SO routing conditions. In each of these figures, the flow-density relationship (i.e., MFD) of the arterials and locals obtained from the simulation are also provided along with their analytical counterparts. Notice that the MFDs of the arterials and locals differ from the analytical estimates, especially in the capacity and congested regimes. This is reasonable and expected in grid simulations, and these features are due to the tendency of the network toward inhomogeneous vehicle distributions when the network reaches capacity and gets congested (Daganzo et al., 2011; Mazloumian et al., 2010). For these reasons, the simulated MFDs under UE and SO routing conditions generally do not match well with the analytical estimates.

Nevertheless, both the UE and SO MFDs obtained from the simulation have properties that match those of the analytically derived MFDs in the free-flow branch of the network. Specifically, the UE MFD exhibits a clear non-concave and non-unimodal pattern in the uncongested regime. By contrast, the SO MFD is concave and unimodal. The right side of Fig. 11a reveals that average network flows in the SO MFD are always higher than those experienced in the UE MFD for the same density. Thus, it appears that the analytical model is able to reveal features of hierarchical network-wide traffic behavior in two-dimensional networks.

The left side of Fig. 11b compares the simulated speeds of arterial and local roads under UE conditions, which explains the cause for the lack of concavity. The minor decrease of arterial speed in the range of $k_H \in (0, 18)$ veh/(lane-mile) corresponds to the first increase of network flow in Fig. 11a where both arterial and local roads are in free flow condition. Then arterial speed drops dramatically in the range of $k_H \in (18, 26)$ veh/(lane-mile) while local road speed does not change. This indicates that the arterials have reached capacity while the local roads are still barely used due to a slower speed. Within this range, the network flow does not change with network density. Thereafter, as speeds of arterials and locals are close, more vehicles start to use local roads, which leads to the second increase of network flow in Fig. 11a. The right side of Fig. 11b compares the simulated speeds of arterial and local roads under SO conditions. Different from the UE condition, the arterial speed decreases slowly with network density while local road speed has already started to decrease at around density of 18. This is because under SO conditions, the capacity of arterials is maintained for as long as possible. This necessitates heavy use of local roads at a low network density, which leads to an early decrease in local road speed.

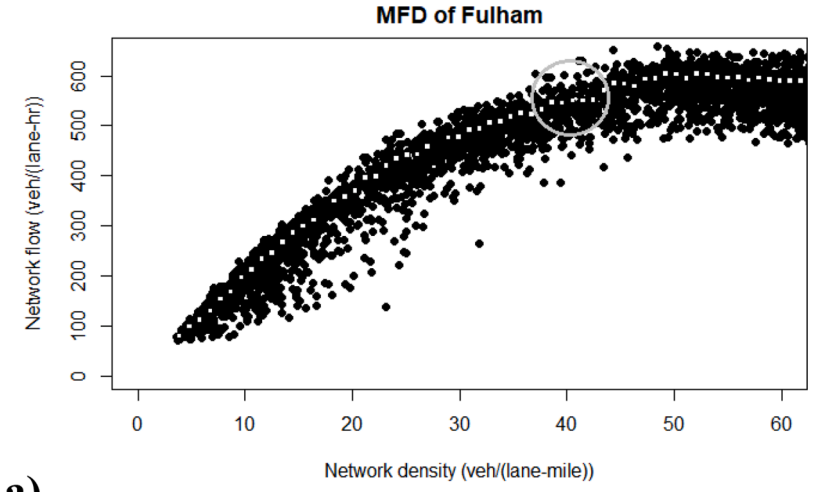

a)

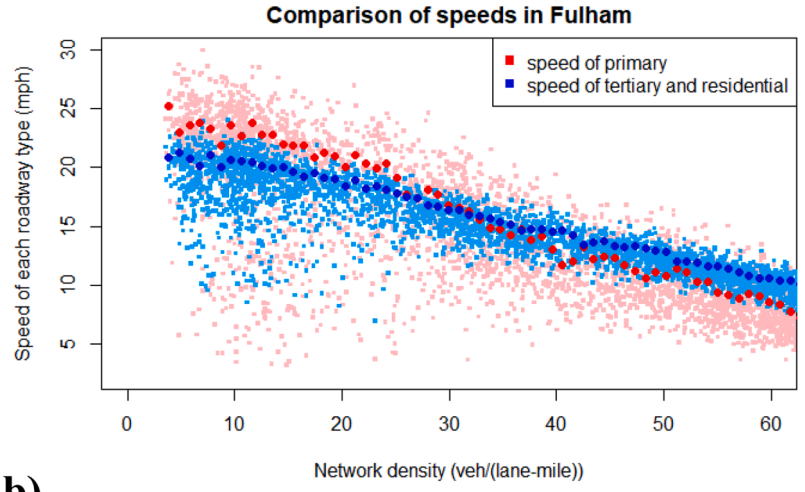

b)

Fig. 13. a) MFD of Fulham, London; b) Comparison of speed of each road type of Fulham, London.

5. Validation of analytical findings

In this section, we revisit the MFDs obtained from the AIMSUN simulation and empirical data from London to determine if the network hierarchy might be the cause of the non-unimodal MFD features that are observed.

The UE routing condition is more in line with what is expected in the real world. Therefore, according to the analytical method and the CAM simulation results, we would expect that the arterial speed will first decrease with network density until it gets close to the local road speed while local road speed barely changes. During this time, network flow will first increase with network density and then will remain unchanged when the arterial reaches capacity. This corresponds to the condition when vehicles mainly use arterials and use local roads only to access arterials or access their destinations. After that, arterial speed and local speed will jointly decrease at the same rate with network density. In this regime, network flow will increase with network density again until the local road reaches capacity.

5.1. *AIMSUN simulations*

The MFD and speeds of each roadway type under different simulated network structures in the middle column of Fig. 1 are shown in Fig. 12. It can be clearly observed that the shapes of all MFDs are similar to the shape of the MFD of the hierarchical network under UE routing conditions in Fig. 10 while the changes of arterial speed and local speed are in line with Fig. 11b.

Looking at the grid hierarchical network of Fig. 12a, it can be observed that the flow increases with density in the range $k_H \in (0, 6)$ veh/(lane-mile) and remains unchanged in the range of $k_H \in (6, 7)$ veh/(lane-mile). This corresponds to the dramatic decrease of

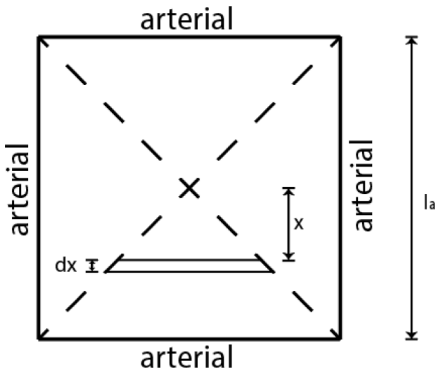

Fig. A1. An "arterial square" from the grid network.

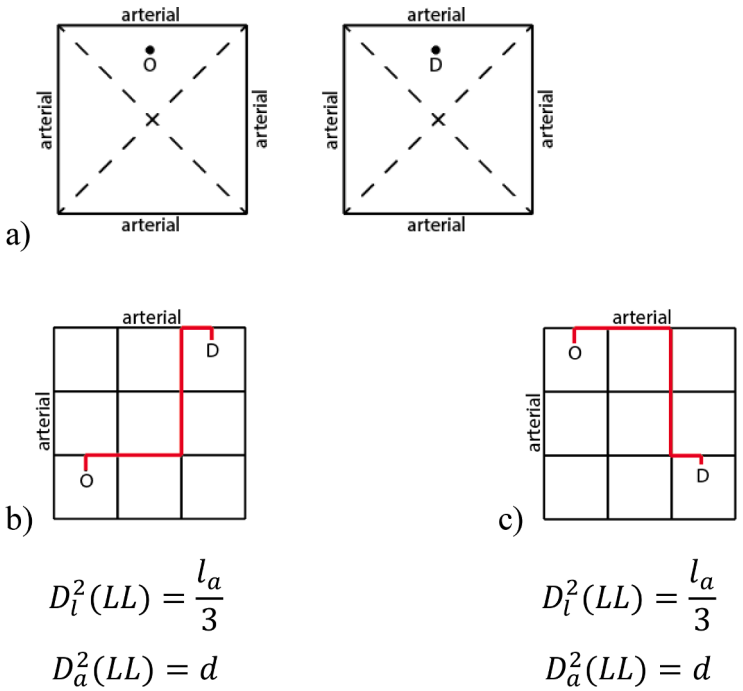

$$D_l^2(LL) = \frac{l_a}{3}$$
$$D_a^2(LL) = d$$

$$D_l^2(LL) = \frac{l_a}{3}$$
$$D_a^2(LL) = d$$

Fig. A2. a) Relative location of OD in the arterial square; b) Relative location of OD in the network: case 1; c) Relative location of OD in the network: case 2.

arterial speed within the same density range in Fig. 12b. The speed of local roads, however, does not change much during this period. At the end of this period, the speed of arterials has dropped to the speed of local roads and thus more vehicles start to use local roads. As a result, the flow increases again with density in the range $k_H \in (7, 15)$ veh/(lane-mile). During this period, the speeds of the two road types are close and change at the same rate with network density. Finally, both arterials and locals reach capacity and the network flow does not change with density again. Similar features can also be observed in the ring and ring-radial hierarchical network of Fig. 12. It is worth noting that the speed of arterial is higher in the ring and ring-radial hierarchical network than in the grid hierarchical network. This is because in these two networks, a higher proportion of arterials is at the border area of the network in which density is lower and speed is faster. As a result, the average speed of arterials in these two networks is higher than the average speed of arterials in the grid hierarchical network.

It is worth mentioning that seemingly non-concave patterns can be sometimes observed even on a single type of road (e.g., density range $k_l \in (24, 30)$ veh/(lane-mile) on local roads in the grid hierarchical network in Fig. 12a). However, these seemingly non-concave patterns are due to randomness. In both simulations and real world, densities at the center area of the network often increase faster than densities at the border area of the network. This uneven density distribution might cause random fluctuations in the network flow for any given network density which sometimes leads to seemingly non-concave patterns even in the MFD of a single type of road. Note that the seemingly non-concave pattern due to randomness is not repeatable in every simulation of the same network while the non-concave pattern in the MFD of the hierarchical network due to UE routing conditions is observed in the same density

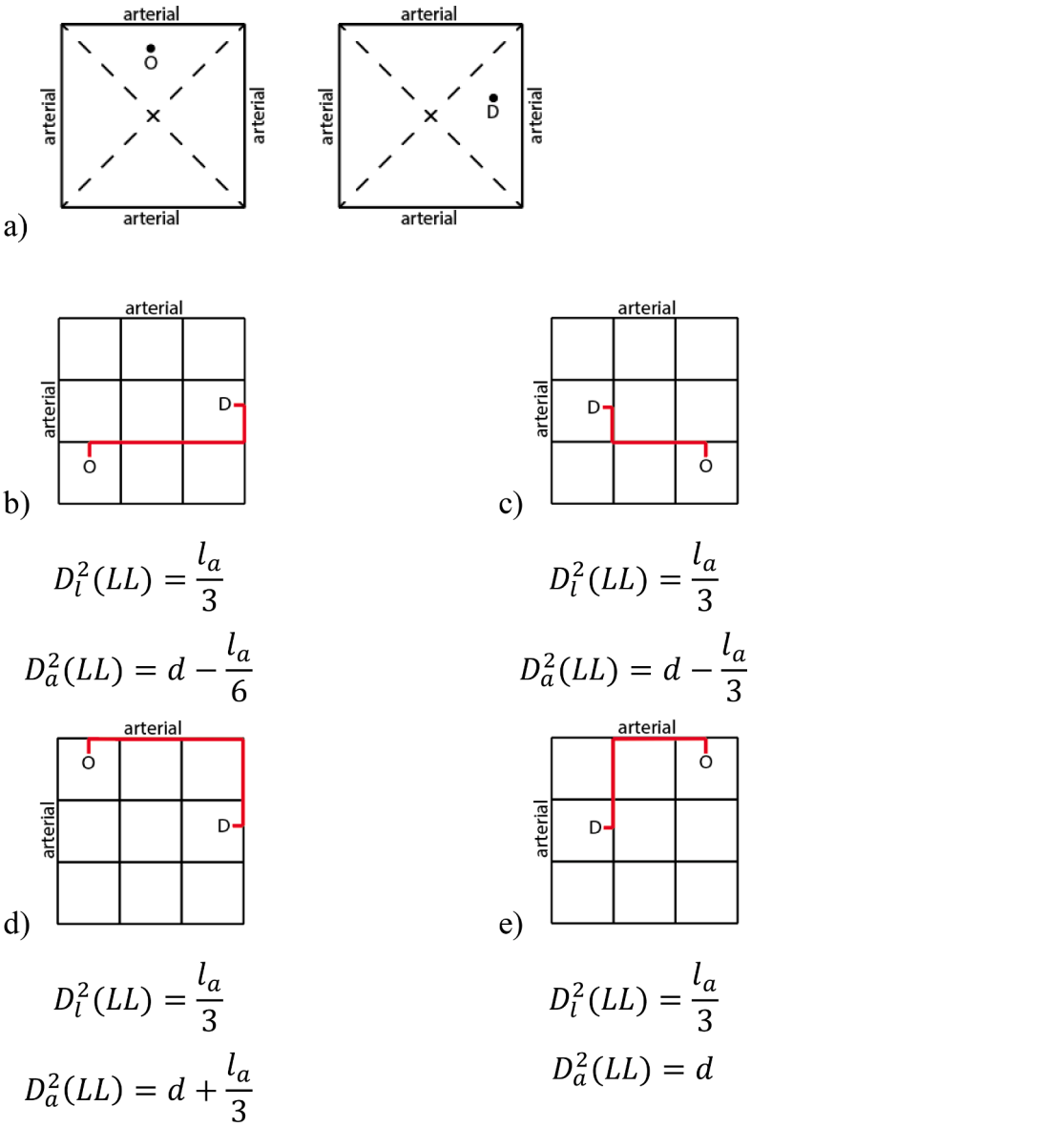

Fig. A3. a) relative location of OD in the arterial square; b) Relative location of OD in the network: case 1; c) Relative location of OD in the network: case 2 d) Relative location of OD in the network: case 3. e) Relative location of OD in the network: case 4.

range in all simulations of the same network.

5.2. Empirical data

Fig. 13a shows the MFD of Fulham, London, which again follows the analytical shape of MFD under UE routing conditions. Fig. 13b compares the speeds on primary roads (red squares) and the speeds on tertiary and residential roads (blue squares). These speeds were obtained from the same methodology as used for the flow-density pairs (white squares) in Fig. 13a. Similar to the simulation results, we can observe that network flow first increases with network density and then remains unchanged for a small range of density, which corresponds to the dramatic decrease of speed of primary roads within the density range of (0,32) veh/(lane-mile) in Fig. 13b. A branch also arises around density of 32 to 50 veh/(lane-mile) where speeds of the two roadway types are close and decrease at the same rate in Fig. 13b. This corresponds to the second increase of network flow in the density range of 43 to 50 veh/(lane-mile) after the non-concave pattern in Fig. 13a. However, the density ranges of the two branches in Fig. 13a and b are not perfectly matched. One potential reason is that primary roads may still be more attractive for trip planning in the real world even if the speed of primary roads is slightly lower than the speed of residential roads. Real drivers likely are not acutely aware of the existing state of arterial roadway congestion, but might gravitate towards arterials as arterials are expected to provide more mobility.

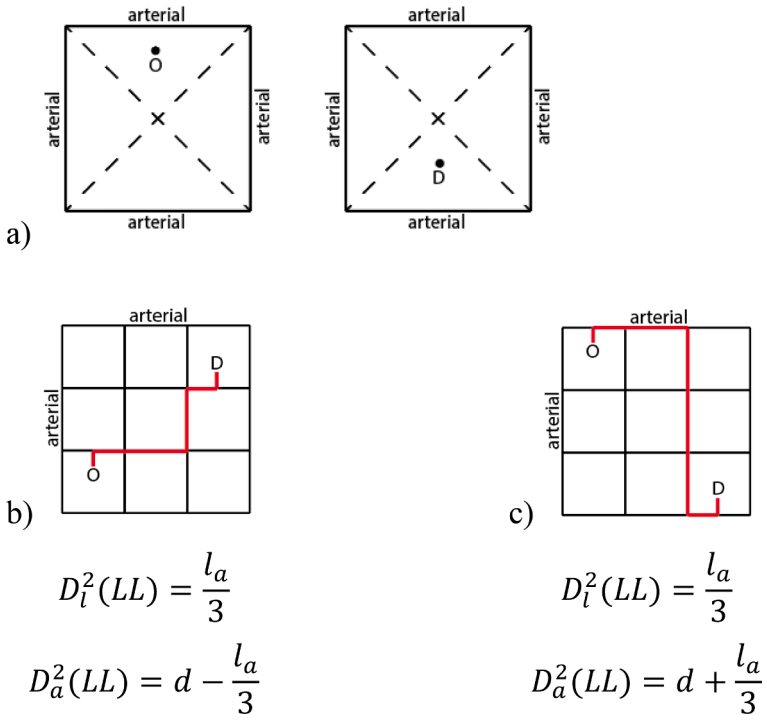

Fig. A4. a) Relative location of OD in the arterial square; b) Relative location of OD in the network: case 1; c) Relative location of OD in the network: case 2.

6. Discussion

This paper examines the influence of hierarchical network structures on the MFDs to better understand the features that should generally be expected in real-world MFDs. An analytical examination was performed on both a simple linear corridor and an idealized two-dimensional grid network to isolate features that are specific to hierarchical network structures. Since the performance of hierarchical networks depends on how users route themselves in the network, the analytical method considers both UE and SO routing conditions. For the linear corridor, the analytical results are compared to MFDs obtained from a cellular automata simulation. The analytical results and the simulation results are found to match up quite well for free-flow and capacity states in both UE and SO routing cases. For the two-dimensional hierarchical network, the non-concave pattern of MFD under UE conditions and the concave pattern of MFD under SO conditions observed from analytical results are also confirmed by the simulation. The use of the analytical method to estimate the impact of roadway hierarchy on the network's MFD is thus validated. Finally, the analytical method was also used to explain the impact of roadway hierarchy on the patterns of MFD observed in a more realistic AIMSUN simulation and the real-world MFD obtained from Fulham, London.

The analytical results reveal interesting findings about the functional form of hierarchical network MFDs. In both the corridor and grid network case, the free-flow branch of the MFDs obtained under UE routing conditions is found to not be unimodal or concave, even though the MFDs of individual street types are unimodal and concave. This lack of concavity can be clearly observed in the linear corridor simulations but is sometimes not as readily observed in the two-dimensional hierarchical network simulations as in the analytical model. This is because congestion in the large-scale network is not always uniformly distributed (as expected), which could mask this non-concave pattern. Moreover, congestion at the boundary of the different street types (e.g., at intersections between arterial and local streets) could limit how easily vehicles are able to move between the two levels.

The non-unimodal nature of the MFDs of hierarchical street networks is important as the assumption of a concave, unimodal MFD is common in almost all MFD modeling frameworks to date. This assumption is then leveraged for optimization purposes and in proofs when developing network-wide traffic control strategies using the MFD. However, the findings here are not necessarily surprising. Most MFDs obtained from empirical data have relatively few data points available when the network is truly congested, even just for specific roadway types. This could lead to inaccurate conclusions about the MFD shape and functional form, especially if multiple peaks exist as would be expected from the findings here. Moreover, most MFDs from empirical data are developed for homogeneous street networks while seldom any research has focused on the MFDs of real-world hierarchical networks. This could be one reason for the lack of observations of the non-concave pattern in the existing literature.

Overall, this paper contributes to the growing literature on relationships between traffic variables aggregated across large spatial regions and how these relationships are influenced by network features. While providing valuable insights, this paper has certain limitations that need to be addressed in future research.

1 This paper only provides analytical estimates of MFDs for networks with simple hierarchical structures. Future work should extend the methodology to more realistic hierarchical networks. In addition, future research should investigate the relationship between the MFD and more general metrics of hierarchical network structures (e.g., degree, closeness, betweenness, and clustering).
2 Certain findings presented in this paper are only derived from simulation experiments. For instance, the simulations revealed that bottlenecks at transition points between roadway types were found to cause non-stationary states. However, this impact of bottlenecks was not analytically modeled in this paper. Therefore, future research should focus on expanding the analytical model to account for these features and potential impacts.
3 The findings reveal that the combination of hierarchical streets and UE routing can lead to non-unimodal patterns in a network's MFD. However, future work should determine whether the presence of hierarchical streets is an essential prerequisite for these non-unimodal MFD patterns (i.e., if non-unimodal patterns may arise without hierarchical network structures).
4 This paper does not consider the impact of routing strategies on the turning ratios at the intersections, which has been shown to influence a network's MFD (Xu et al., 2020). Therefore, additional work is also needed to understand how route choice will impact turning movements at intersections and consider this combined impact on a network's MFD.
5 Finally, future work should examine the impact of trip distance on the non-unimodal nature of the MFDs of hierarchical street networks. It is possible that shorter trip distances may diminish the impact of routing, which could potentially conceal the non-unimodal pattern.

CRediT authorship contribution statement

Guanhao Xu: Conceptualization, Methodology, Formal analysis, Writing – review & editing. **Vikash V. Gayah:** Conceptualization, Methodology, Formal analysis, Writing – review & editing.

Acknowledgments

This manuscript has been authored in part by UT-Battelle, LLC, under contract DE-AC05-00OR22725 with the US Department of Energy (DOE). The publisher acknowledges the US government license to provide public access under the DOE Public Access Plan (http://energy.gov/downloads/doe-public-access-plan). This research was supported by NSF Grant CMMI-1749200.

Appendix A

This appendix provides the derivation of average distance on local roads and arterials for the OD pair LL under routing strategy 2, $D_l^2(LL)$ and $D_a^2(LL)$. The same process can be performed to get the values of other $D_i^j(z),\ i = a\ or\ l,\ j = 1\ or\ 2,\ z = LL,\ LA,\ AL\ or\ AA$.

To get the trip distance of each routing option, we need to first derive the average distance from the origin/destination to the nearest arterial. For simplicity, we first assume that the local roads are infinitely dense so that ODs are uniformly distributed in the spatial space. Then let's take one "arterial square" (with arterials being the four edges) from the grid network and divide it into four triangles, as shown in Fig. A1. The hypotenuse of each triangle is the nearest arterial from the ODs within the triangle. Noting that the four triangles are exactly the same, we only have to consider one of them.

Since ODs are uniformly located in each triangle, we can calculate the mean distance to the nearest arterial (denoted by μ_d) using the following equation:

$$\mu_d = \sum p_i.l_i \tag{11}$$

where p_i is the possibility that an origin or destination is located at point i and l_i is the distance from the origin or destination located at point i to the nearest arterial or the nearest edge of the square.

In Fig. A1, when dx is very small, the distance from all ODs located in the trapezoid to the nearest arterial is $\frac{l_a}{2} - x$. Meanwhile, when dx is very small, the trapezoid can be seen as a rectangle with an area of $2xdx$. Therefore, we calculate μ_d by:

$$\mu_d = \sum p_i.l_i = \int_0^{\frac{l_a}{2}} \frac{Area_{\text{trapezoid}}}{Area_{triangle}} \times \left(\frac{l_a}{2} - x\right) = \int_0^{\frac{l_a}{2}} \frac{2x.dx}{\frac{l_a^2}{4}} \times \left(\frac{l_a}{2} - x\right) = \frac{l_a}{6} \tag{12}$$

Then we will use μ_d to determine $D_l^2(LL)$ and $D_a^2(LL)$ which depend on the relative location of OD. The relative location of OD is important because in some cases, there will be additional trip distance due to routing (accessing the nearest arterial from the origin or the destination) while in other cases, the distance from origin/destination to the nearest arterial can be part of the shortest path and thus there will be no additional trip distance due to routing. In light of this, three relative locations of OD in the "arterial square" is considered (Figs. A2-A4): a. OD locate in the same triangles of the "arterial square" (probability of 0.25) b. OD locate in the abutting triangles of the "arterial square" (probability of 0.5) c. OD locate in the opposite triangles of the "arterial square" (probability of 0.25)

Considering all the cases with their possibilities, the average distance on locals $D_l^2(LL)$ and the average distance on arterials $D_a^2(LL)$ for OD pair LL under routing option 2 are:

$$D_l^2(LL) = \frac{l_a}{3} \tag{13}$$

$$\begin{aligned} D_a^2(LL) &= 0.25\mathrm{d} + 0.5 \times \left(0.25 \times \left(d - \frac{l_a}{6}\right) + 0.25 \times \left(d - \frac{l_a}{3}\right) + 0.25 \times \left(d + \frac{l_a}{3}\right) + 0.25 \times d\right) \; + 0.25 \\ &\quad \times \left(0.5 \times \left(d - \frac{l_a}{3}\right) + 0.5 \times \left(d + \frac{l_a}{3}\right)\right) \\ &= d - \frac{l_a}{48} \end{aligned} \tag{14}$$

References

Aboudolas, K., Geroliminis, N., 2013. Perimeter and boundary flow control in multi-reservoir heterogeneous networks. Transp. Res. Part B Methodol. 55, 265–281.

Aghamohammadi, R., Laval, J.A., 2022. Parameter estimation of the macroscopic fundamental diagram: a maximum likelihood approach. Transp. Res. Part C Emerg. Technol. 140, 103678.

Ambühl, L., Loder, A., Bliemer, M.C.J., Menendez, M., Axhausen, K.W., 2018. Introducing a re-sampling methodology for the estimation of empirical macroscopic fundamental diagrams. Transp. Res. Rec. 2672, 239–248.

Ambühl, L., Loder, A., Leclercq, L., Menendez, M., 2021. Disentangling the city traffic rhythms: a longitudinal analysis of MFD patterns over a year. Transp. Res. Part C Emerg. Technol. 126, 103065.

Ambühl, L., Loder, A., Zheng, N., Axhausen, K.W., Menendez, M., 2019. Approximative network partitioning for MFDs from stationary sensor data. Transp. Res. Rec. 2673, 94–103.

Ambühl, L., Menendez, M., 2016. Data fusion algorithm for macroscopic fundamental diagram estimation. Transp. Res. Part C Emerg. Technol. 71, 184–197.

Ampountolas, K., Kouvelas, A., 2015. Real-time estimation of critical values of the macroscopic fundamental diagram for maximum network throughput. TRB 94th Annual Meeting Compendium of Papers, pp. 15–1779.

Bazzani, A., Giorgini, B., Gallotti, R., Giovannini, L., Marchioni, M., Rambaldi, S., 2011. Towards congestion detection in transportation networks using GPS data. In: Proc. - 2011 IEEE Int. Conf. Privacy, Secur. Risk Trust IEEE Int. Conf. Soc. Comput. PASSAT/SocialCom 2011, pp. 1455–1459.

Buisson, C., Ladier, C., 2009. Exploring the impact of homogeneity of traffic measurements on the existence of macroscopic fundamental diagrams. Transp. Res. Rec. 127–136.

Cascetta, E., Nuzzolo, A., Russo, F., Vitetta, A., 1996. A modified logit route choice model overcoming path overlapping problems. Specification and some calibration results for interurban networks. In: Transportation and Traffic Theory. Proceedings of The 13th International Symposium On Transportation And Traffic Theory. Lyon, France.

Coifman, B., 2001. Improved velocity estimation using single loop detectors. Transp. Res. Part A Policy Pract. 35, 863–880.

Courbon, T., Leclercq, L., 2011. Cross-comparison of macroscopic fundamental diagram estimation methods. Procedia - Soc. Behav. Sci. 20, 417–426.

Daganzo, C.F., 2010. Public transportation systems: basic principles of system design. Operations Planning and Real-TimeControl.

Daganzo, C.F., 2007. Urban gridlock: macroscopic modeling and mitigation approaches. Transp. Res. Part B Methodol. 41, 49–62.

Daganzo, C.F., 2006. In traffic flow, cellular automata = kinematic waves. Transp. Res. Part B Methodol. 40, 396–403.

Daganzo, C.F., 2005. A variational formulation of kinematic waves: basic theory and complex boundary conditions. Transp. Res. Part B Methodol. 39, 187–196.

Daganzo, C.F., Gayah, V.V., Gonzales, E.J., 2011. Macroscopic relations of urban traffic variables: bifurcations, multivaluedness and instability. Transp. Res. Part B Methodol. 45, 278–288.

Daganzo, C.F., Geroliminis, N., 2008. An analytical approximation for the macroscopic fundamental diagram of urban traffic. Transp. Res. Part B Methodol. 42, 771–781.

Daganzo, C.F., Lehe, L.J., 2016. Traffic flow on signalized streets. Transp. Res. Part B Methodol. 90, 56–69.

Daganzo, C.F., Menendez, M., 2005. A variational formulation of kinematic waves: bottleneck properties and examples. In: Transportation and Traffic Theory. Flow, Dynamics and Human Interaction. 16th International Symposium on Transportation and Traffic TheoryUniversity of Maryland. College Park.

Dakic, I., Ambühl, L., Schümperlin, O., Menendez, M., 2020. On the modeling of passenger mobility for stochastic bi-modal urban corridors. Transp. Res. Part C Emerg. Technol. 113, 146–163.

Deprator, A.J., Hitchcock, O., Gayah, V.V., 2017. Improving urban street network efficiency by prohibiting conflicting left turns at signalized intersections. Transp. Res. Rec. 2622, 58–69.

Du, J., Rakha, H., Gayah, V.V., 2016. Deriving macroscopic fundamental diagrams from probe data: issues and proposed solutions. Transp. Res. Part C Emerg. Technol. 66, 136–149.

Edie, L.C., 1965. Discussion of traffic stream measurements and definitions. In: 2nd International Symposium on the Theory of Traffic Flow, pp. 139–154.

Fu, H., Wang, Y., Tang, X., Zheng, N., Geroliminis, N., 2020. Empirical analysis of large-scale multimodal traffic with multi-sensor data. Transp. Res. Part C Emerg. Technol. 118, 102725.

Gayah, V., Dixit, V., 2013. Using mobile probe data and the macroscopic fundamental diagram to estimate network densities. Transp. Res. Rec. 76–86.

Gayah, V.V., Daganzo, C.F., 2011. Clockwise hysteresis loops in the macroscopic fundamental diagram: an effect of network instability. Transp. Res. Part B Methodol. 45, 643–655.

Gayah, V.V., Gao, X., Nagle, A.S., 2014. On the impacts of locally adaptive signal control on urban network stability and the macroscopic fundamental diagram. Transp. Res. Part B Methodol. 70, 255–268.

Geroliminis, N., Boyaci, B., 2012. The effect of variability of urban systems characteristics in the network capacity. Transp. Res. Part B Methodol. 46, 1607–1623.

Geroliminis, N., Daganzo, C.F., 2008. Existence of urban-scale macroscopic fundamental diagrams: some experimental findings. Transp. Res. Part B Methodol. 42, 759–770.

Geroliminis, N., Haddad, J., Ramezani, M., 2013. Optimal perimeter control for two urban regions with macroscopic fundamental diagrams: a model predictive approach. IEEE Trans. Intell. Transp. Syst. 14, 348–359.

Geroliminis, N., Sun, J., 2011. Properties of a well-defined macroscopic fundamental diagram for urban traffic. Transp. Res. Part B Methodol. 45, 605–617.

Godfrey, J.W., 1969. The mechanism of a road network. Traffic Eng. Control 11 (7), 323–327.

Gonzales, E.J., Daganzo, C.F., 2013. The evening commute with cars and transit: duality results and user equilibrium for the combined morning and evening peaks. Procedia - Soc. Behav. Sci. 80, 249–265.

Gonzales, E.J., Daganzo, C.F., 2012. Morning commute with competing modes and distributed demand: user equilibrium, system optimum, and pricing. Transp. Res. Part B Methodol. 46, 1519–1534.

Gu, Z., Shafiei, S., Liu, Z., Saberi, M., 2018. Optimal distance- and time-dependent area-based pricing with the network fundamental diagram. Transp. Res. Part C Emerg. Technol. 95, 1–28.

Haddad, J., 2017. Optimal perimeter control synthesis for two urban regions with aggregate boundary queue dynamics. Transp. Res. Part B Methodol. 96, 1–25.
Haitao, H., Yang, K., Liang, H., Menendez, M., Guler, S.I., 2019. Providing public transport priority in the perimeter of urban networks: a bimodal strategy. Transp. Res. Part C Emerg. Technol. 107, 171–192.
Hans, E., Chiabaut, N., Leclercq, L., 2015. Applying variational theory to travel time estimation on urban arterials. Transp. Res. Part B Methodol. 78, 169–181.
Hong, R., Liu, H., An, C., Wang, B., Lu, Z., Xia, J., 2022. An MFD construction method considering multi-source data reliability for urban road networks. Sustainability 14, 6188.
Huang, C., Zheng, N., Zhang, J., 2019. Investigation of bimodal macroscopic fundamental diagrams in large-scale urban networks: empirical study with GPS data for Shenzhen City. Transp. Res. Rec. 2673, 114–128.
Huang, Y., Sun, D., Li, A., Axhausen, K.W., 2021. Impact of bicycle traffic on the macroscopic fundamental diagram: some empirical findings in Shanghai. Transp. A Transp. Sci. 17, 1122–1149.
Ji, Y., Luo, J., Geroliminis, N., 2014. Empirical observations of congestion propagation and dynamic partitioning with probe data for large-scale systems. Transp. Res. Rec. J. Transp. Res. Board 2422, 1–11.
Johari, M., Keyvan-Ekbatani, M., Leclercq, L., Ngoduy, D., Mahmassani, H.S., 2021. Macroscopic network-level traffic models: bridging fifty years of development toward the next era. Transp. Res. Part C Emerg. Technol. 131, 103334.
Keyvan-Ekbatani, M., Kouvelas, A., Papamichail, I., Papageorgiou, M., 2012. Exploiting the fundamental diagram of urban networks for feedback-based gating. Transp. Res. Part B Methodol. 46, 1393–1403.
Keyvan-Ekbatani, M., Papageorgiou, M., Papamichail, I., 2013. Urban congestion gating control based on reduced operational network fundamental diagrams. Transp. Res. Part C Emerg. Technol. 33, 74–87.
Knoop, V., Hoogendoorn, S., 2013. Empirics of a generalized macroscopic fundamental diagram for urban freeways. Transp. Res. Rec. 133–141.
Knoop, V.L., De Jong, D., Hoogendoorn, S.P., 2014. Influence of road layout on network fundamental diagram. Transp. Res. Rec. 2421, 22–30.
Knoop, V.L., Van Erp, P.B.C., Leclercq, L., Hoogendoorn, S.P., 2018. Empirical MFDs using Google traffic data. In: IEEE Conf. Intell. Transp. Syst. Proceedings, ITSC 2018-Novem, pp. 3832–3839.
Laval, J.A., Castrillón, F., 2015. Stochastic approximations for the macroscopic fundamental diagram of urban networks. Transp. Res. Part B Methodol. 81, 904–916.
Leclercq, L., Chiabaut, N., Trinquier, B., 2014. Macroscopic fundamental diagrams: a cross-comparison of estimation methods. Transp. Res. Part B Methodol. 62, 1–12.
Leclercq, L., Geroliminis, N., 2013. Estimating MFDs in simple networks with route choice. Transp. Res. Part B Methodol. 57, 468–484.
Li, J., Xie, N., Zhang, K., Guo, F., Hu, S., (Michael) Chen, X., 2022. Network-scale traffic prediction via knowledge transfer and regional MFD analysis. Transp. Res. Part C Emerg. Technol. 141, 103719.
Lighthill, M.J., Whitham, G.B., 1955a. On kinematic waves II. A theory of traffic flow on long crowded roads. Proc. R. Soc. London. Ser. A. Math. Phys. Sci. 229, 317–345.
Lighthill, M.J., Whitham, G.B., 1955b. On kinematic waves I. Flood movement in long rivers. Proc. R. Soc. London. Ser. A. Math. Phys. Sci. 229, 281–316.
Loder, A., Ambühl, L., Menendez, M., Axhausen, K.W., 2019. Understanding traffic capacity of urban networks. Sci. Rep. 9, 16283.
Loder, A., Ambühl, L., Menendez, M., Axhausen, K.W., 2017. Empirics of multi-modal traffic networks – using the 3D macroscopic fundamental diagram. Transp. Res. Part C Emerg. Technol. 82, 88–101.
Loder, A., Bliemer, M.C.J., Axhausen, K.W., 2022. Optimal pricing and investment in a multi-modal city — introducing a macroscopic network design problem based on the MFD. Transp. Res. Part A Policy Pract. 156, 113–132.
Mahmassani, H., Williams, J.C., Herman, R., 1984. Investigation of network-level traffic flow relationships: some simulation results. Transp. Res. Rec. 121–130.
Mahmassani, H.S., Williams, J.C., Hennan, R., 1987. Performance of urban traffic networks performance of urban traffic networks. In: The 10th International Symposium on Transportation and Traffic Theory. Amsterdam, The Netherlands, Vol. 14. Elsevier, pp. 1–20.
Mazloumian, A., Geroliminis, N., Helbing, D., 2010. The spatial variability of vehicle densities as determinant of urban network capacity. Philos. Trans. R. Soc. A Math. Phys. Eng. Sci. 368, 4627–4647.
Mühlich, N., Gayah, V.V., Menendez, Monica, 2015. An examination of MFD hysteresis patterns for hierarchical urban street networks using micro-simulation. Transp. Res. Rec. 2491, 117–126.
Nagle, A.S., Gayah, V.V., 2014. Accuracy of networkwide traffic states estimated from mobile probe data. Transp. Res. Rec. J. Transp. Res. Board 2421, 1–11.
Ortigosa, J., Gayah, V.V., Menendez, M., 2019. Analysis of one-way and two-way street configurations on urban grid networks. Transp. B 7, 61–81.
Ortigosa, J., Menendez, M., 2014. Traffic performance on quasi-grid urban structures. Cities 36, 18–27.
Paipuri, M., Barmpounakis, E., Geroliminis, N., Leclercq, L., 2021. Empirical observations of multi-modal network-level models: insights from the pNEUMA experiment. Transp. Res. Part C Emerg. Technol. 131, 103300.
Paipuri, M., Xu, Y., González, M.C., Leclercq, L., 2020. Estimating MFDs, trip lengths and path flow distributions in a multi-region setting using mobile phone data. Transp. Res. Part C Emerg. Technol. 118, 102709.
Ren, Y., Hou, Z., Sirmatel, I.I., Geroliminis, N., 2020. Data driven model free adaptive iterative learning perimeter control for large-scale urban road networks. Transp. Res. Part C Emerg. Technol. 115, 102618.
Richards, P.I., 1956. Shock waves on the highway. Oper. Res. 4, 42–51.
Saberi, M., Mahmassani, H.S., Zockaie, A., 2014. Network capacity, traffic instability, and adaptive driving: findings from simulated urban network experiments. EURO J. Transp. Logist. 3, 289–308.
Saffari, E., Yildirimoglu, M., Hickman, M., 2022. Data fusion for estimating macroscopic fundamental diagram in large-scale urban networks. Transp. Res. Part C Emerg. Technol. 137, 103555.
Saffari, E., Yildirimoglu, M., Hickman, M., 2020. A methodology for identifying critical links and estimating macroscopic fundamental diagram in large-scale urban networks. Transp. Res. Part C Emerg. Technol. 119, 102743.
Shim, J., Yeo, J., Lee, S., Hamdar, S.H., Jang, K., 2019. Empirical evaluation of influential factors on bifurcation in macroscopic fundamental diagrams. Transp. Res. Part C Emerg. Technol. 102, 509–520.
Simoni, M.D., Pel, A.J., Waraich, R.A., Hoogendoorn, S.P., 2015. Marginal cost congestion pricing based on the network fundamental diagram. Transp. Res. Part C Emerg. Technol. 56, 221–238.
Tilg, G., Ambühl, L., Batista, S., Menendez, M., Busch, F., 2021. On the application of variational theory to urban networks. Transp. Res. Part B Methodol. 150, 435–456.
Tilg, G., Amini, S., Busch, F., 2020. Evaluation of analytical approximation methods for the macroscopic fundamental diagram. Transp. Res. Part C Emerg. Technol. 114, 1–19.
Tsubota, T., Bhaskar, A., Chung, E., 2014. Macroscopic fundamental diagram for Brisbane, Australia. Transp. Res. Rec. J. Transp. Res. Board 2421, 12–21.
Wang, P.fei, Wada, K., Akamaysu, T., Hara, Y., 2015. An empirical analysis of macroscopic fundamental diagrams for Sendai road networks. Interdiscip. Inf. Sci. 21, 49–61.
Wardrop, J.G., 1952. Some theoretical aspects of road traffic research. In: ICE Proceedings: Engineering Divisions, pp. 325–362.
Xu, G., Yu, Z., Gayah, V.V., 2020. Analytical method to approximate the impact of turning on the macroscopic fundamental diagram. Transp. Res. Rec. 2674, 933–947.
Yang, K., Menendez, M., Zheng, N., 2019. Heterogeneity aware urban traffic control in a connected vehicle environment: a joint framework for congestion pricing and perimeter control. Transp. Res. Part C Emerg. Technol. 105, 439–455.

Yildirimoglu, M., Sirmatel, I.I., Geroliminis, N., 2018. Hierarchical control of heterogeneous large-scale urban road networks via path assignment and regional route guidance. Transp. Res. Part B Methodol. 118, 106–123.
Zheng, N., Rérat, G., Geroliminis, N., 2016. Time-dependent area-based pricing for multimodal systems with heterogeneous users in an agent-based environment. Transp. Res. Part C Emerg. Technol. 62, 133–148.
Zheng, N., Waraich, R.A., Axhausen, K.W., Geroliminis, N., 2012. A dynamic cordon pricing scheme combining the macroscopic fundamental diagram and an agent-based traffic model. Transp. Res. Part A Policy Pract. 46, 1291–1303.